

1

2 **Mosaic cis-regulatory evolution drives transcriptional partitioning of**  
3 **HERVH endogenous retrovirus in the human embryo**

4

5 Thomas A. Carter<sup>1</sup>, Manvendra Singh<sup>1</sup>, Gabrijela Dumbović<sup>2,3</sup>, Jason D. Chobirko<sup>1</sup>,  
6 John L. Rinn<sup>2</sup>, Cédric Feschotte<sup>1\*</sup>

7 \*: corresponding author

8

9 1) Department of Molecular Biology and Genetics, Cornell University, Ithaca, NY 14850, USA

10 2) Department of Biochemistry, University of Colorado Boulder, Boulder, CO 80309, USA

11 3) Present address: Max Planck Institute of Immunobiology and Epigenetics, Freiburg, Germany

## 12 **Abstract**

13 The human endogenous retrovirus type-H (HERVH) family is expressed in the  
14 preimplantation embryo. A subset of these elements are specifically transcribed in  
15 pluripotent stem cells where they appear to exert regulatory activities promoting self-  
16 renewal and pluripotency. How HERVH elements achieve such transcriptional  
17 specificity remains poorly understood. To uncover the sequence features underlying  
18 HERVH transcriptional activity, we performed a phyloregulatory analysis of the long  
19 terminal repeats (LTR7) of the HERVH family, which harbor its promoter, using a wealth  
20 of regulatory genomics data. We found that the family includes at least 8 previously  
21 unrecognized subfamilies that have been active at different timepoints in primate  
22 evolution and display distinct expression patterns during human embryonic  
23 development. Notably, nearly all HERVH elements transcribed in ESCs belong to one of  
24 the youngest subfamilies we dubbed LTR7up. LTR7 sequence evolution was driven by  
25 complex mutational processes, including multiple recombination events between  
26 subfamilies, that led to transcription factor binding motif modules characteristic of each  
27 subfamily. Using a reporter assay, we show that one such motif, a predicted SOX2/3  
28 binding site unique to LTR7up, is essential for robust promoter activity in induced  
29 pluripotent stem cells. Together these findings illuminate the mechanisms by which  
30 HERVH diversified its expression pattern during evolution to colonize distinct cellular  
31 niches within the human embryo.

## 32 **Introduction**

33 Transposable elements (TEs) are genomic parasites that use the host cell machinery  
34 for their own propagation. To propagate in the host genome, they must generate new  
35 insertions in germ cells or their embryonic precursors, as to be passed on to the next  
36 generation (Charlesworth and Langley, 1986; Cosby et al., 2019; Haig, 2016). To this  
37 end, many TEs have evolved stage-specific expression in germ cells or early embryonic  
38 development (Faulkner et al., 2009; Fort et al., 2014; Göke et al., 2015; Miao et al.,  
39 2020; Urusov et al., 2011). But how does this precise control of TE expression evolve?

40 Many endogenous retroviruses (ERVs) are known to exhibit highly stage-specific  
41 expression during early embryonic development (Chang et al., 2021; Göke et al., 2015;  
42 Hermant and Torres-Padilla, 2021; Peaston et al., 2004; Svoboda et al., 2004). ERVs  
43 are derived from exogenous retroviruses with which they share the same prototypical  
44 structure with two long terminal repeats (LTRs) flanking an internal region encoding  
45 products promoting their replication (Eickbush and Malik, 2002). There are hundreds of  
46 ERV families and subfamilies in the human genome, each associated to unique LTR  
47 sequences (Kojima, 2018; Vargiu et al., 2016). Each family has infiltrated the germline  
48 at different evolutionary timepoints and have achieved various levels of genomic  
49 amplification (Bannert and Kurth, 2004; Vargiu et al., 2016). One of the most abundant  
50 families is HERVH, a family derived from a gamma retrovirus that first entered the  
51 genome of the common ancestor of apes, Old World monkeys, and New World  
52 monkeys more than 40 million years ago (mya) (Goodchild et al., 1993; Izsvák et al.,  
53 2016; Mager and Freeman, 1995).

54 There are four subfamilies of HERVH elements currently recognized in the Dfam (Storer  
55 et al., 2021) and Repbase (Bao et al., 2015; Kojima, 2018) databases and annotated in  
56 the reference human genome based on distinct LTR consensus sequences: LTR7  
57 (formerly known as Type I), 7b (Type II), 7c, and 7y (Type Ia) (Bao et al., 2015;  
58 Goodchild et al., 1993; Jern et al., 2005, 2004). Additional subdivisions of HERVH  
59 elements were also proposed based on phylogenetic analysis and structural variation of  
60 their internal gene sequences (Gemmell et al., 2019; Jern et al., 2005, 2004). However,  
61 all HERVH elements are currently annotated in the human genome using a single

62 consensus sequence for the internal region (HERVH\_int) and the aforementioned four  
63 LTR subfamilies.

64 HERVH has been the focus of extensive genomic investigation for its high level of RNA  
65 expression in human embryonic stem cells (ESCs) and induced pluripotent stem cells  
66 (iPSCs) (Fort et al., 2014; Gemmell et al., 2015; Izsvák et al., 2016; Kelley and Rinn,  
67 2012; Loewer et al., 2010; Römer et al., 2017; Santoni et al., 2012; Zhang et al., 2019).  
68 Several studies showed that family-wide HERVH knockdown results in the loss of  
69 pluripotency of human ESC and reduced reprogramming efficiency of somatic cells to  
70 iPSC (Lu et al., 2014; Ohnuki et al., 2014; Wang et al., 2014). Others reported similar  
71 phenotypes with the knockdown of individual HERVH-derived RNAs such as those  
72 produced from the *lincRNA-RoR* and *ESRG* loci (Loewer et al., 2010; Wang et al.,  
73 2014) or the deletion of individual HERVH loci acting as boundaries for topological  
74 associated domains (Zhang et al., 2019). These results converge on the notion that  
75 HERVH products (RNA or proteins) exert some modulatory effect on the cellular  
76 homeostasis of pluripotent stem cells. However, it is important to emphasize that  
77 different HERVH knockdown constructs produced variable results and inconsistent  
78 phenotypes (Lu et al., 2014; Wang et al., 2014; Zhang et al., 2019), and a recent  
79 knockout experiment of the most highly transcribed locus (*ESRG*) failed to recapitulate  
80 its previous knockdown phenotype (Takahashi et al., 2021). Despite intense study,  
81 which expressed HERVH loci, if any, are necessary for the maintenance of pluripotency  
82 remain unclear.

83 The mechanisms regulating the transcription of HERVH also remain poorly understood.  
84 RNA-seq analyses have established that HERVH expression in human ESCs, iPSCs,  
85 and the pluripotent epiblast can be attributed to a relatively small subset of loci  
86 (estimated between 83 and 209) driven by LTR7 (*sensu stricto*) sequences (Göke et al.,  
87 2015; Wang et al., 2014; Zhang et al., 2019). The related 7y sequences are known to  
88 be expressed in the pluripotent epiblast of human embryos (Göke et al., 2015) and a  
89 distinct subset of elements associated with 7b and 7y sequences are expressed even  
90 earlier in development at the onset of embryonic genome activation (Göke et al., 2015).  
91 These observations suggest that the HERVH family is composed of subsets of elements

92 expressed at different timepoints during embryonic development and that these  
93 expression patterns reflect, at least in part, the unique cis-regulatory activities of their  
94 LTRs. While it has been reported that several transcription factors (TFs) bind and  
95 activate HERVH LTRs, including the pluripotency factors OCT4, NANOG, SP1, and  
96 SOX2 (Göke et al., 2015; Ito et al., 2017; Kelley and Rinn, 2012; Kunarso et al., 2010;  
97 Ohnuki et al., 2014; Pontis et al., 2019; Santoni et al., 2012), it remains unclear how TF  
98 binding contributes to the differential expression of HERVH subfamilies and why only a  
99 minority of HERVH are robustly transcribed in pluripotent stem cells and embryonic  
100 development.

101 To shed light on these questions, we focused this study on the cis-regulatory evolution  
102 of LTR7 elements. We use a “phyloregulatory” approach combining phylogenetic  
103 analyses and regulatory genomics to investigate the sequence determinants underlying  
104 the partitioning of expression of HERVH/LTR7 subfamilies during early embryonic  
105 development.

## 106 **Results**

### 107 **LTR7 consists of 8 previously undefined subfamilies**

108 We began our investigation by examining the sequence relationships of the four LTR7  
109 subfamilies currently recognized in the human genome: LTR7 sensu stricto (748 proviral  
110 copies; 711 solo LTRs), 7b (113; 524), 7c (24; 223), and 7y (77; 77). We built a  
111 maximum likelihood phylogenetic tree from a multiple sequence alignment of a total of  
112 781 5' LTR and 1073 solo LTR sequences of near complete length (>350 bp)  
113 representing all intact LTR subfamilies extracted from the RepeatMasker output of the  
114 hg38 human reference assembly. While 7b and 7y sequences cluster, as expected, into  
115 clear monophyletic clades with relatively short internode distances and little subclade  
116 structure, sequences from the 7c and LTR7 subfamilies were much more  
117 heterogeneous and formed many subclades (Fig. 1A). Notably, sequences annotated  
118 as LTR7 were split into distinct monophyletic clades indicative of previously  
119 unrecognized subfamilies within that group. The branch length separating some of  
120 these LTR7 subclades were longer from one another than they were from those falling  
121 within the 7b, 7c, and 7y clades, indicating that they represent subfamilies as different  
122 from each other as those previously recognized (Fig. 1A).

123 We next sought to classify LTR7 elements more finely by performing a phylogenetic  
124 analysis using a multiple sequence alignment of all intact LTR7 sequences (>350 bp)  
125 along with the consensus sequences for the other LTR7 subfamilies for reference. We  
126 defined high-confidence subfamilies as those forming a clade supported by >95%  
127 ultrafast bootstrap (UFbootstrap) and internal branches >0.015 (1.5 nucleotide  
128 substitutions per 100 bp) separating subgroup nodes. Based on these criteria, LTR7  
129 elements could be divided into 8 subfamilies (Fig. 1B).

130 While long internal branches with high UFbootstrap support separate LTR7 subfamilies,  
131 intra-subfamily internal branches with >95% UFbootstrap support were shorter (<0.015),  
132 suggesting that each subfamily was the product of a rapid burst of amplification of a

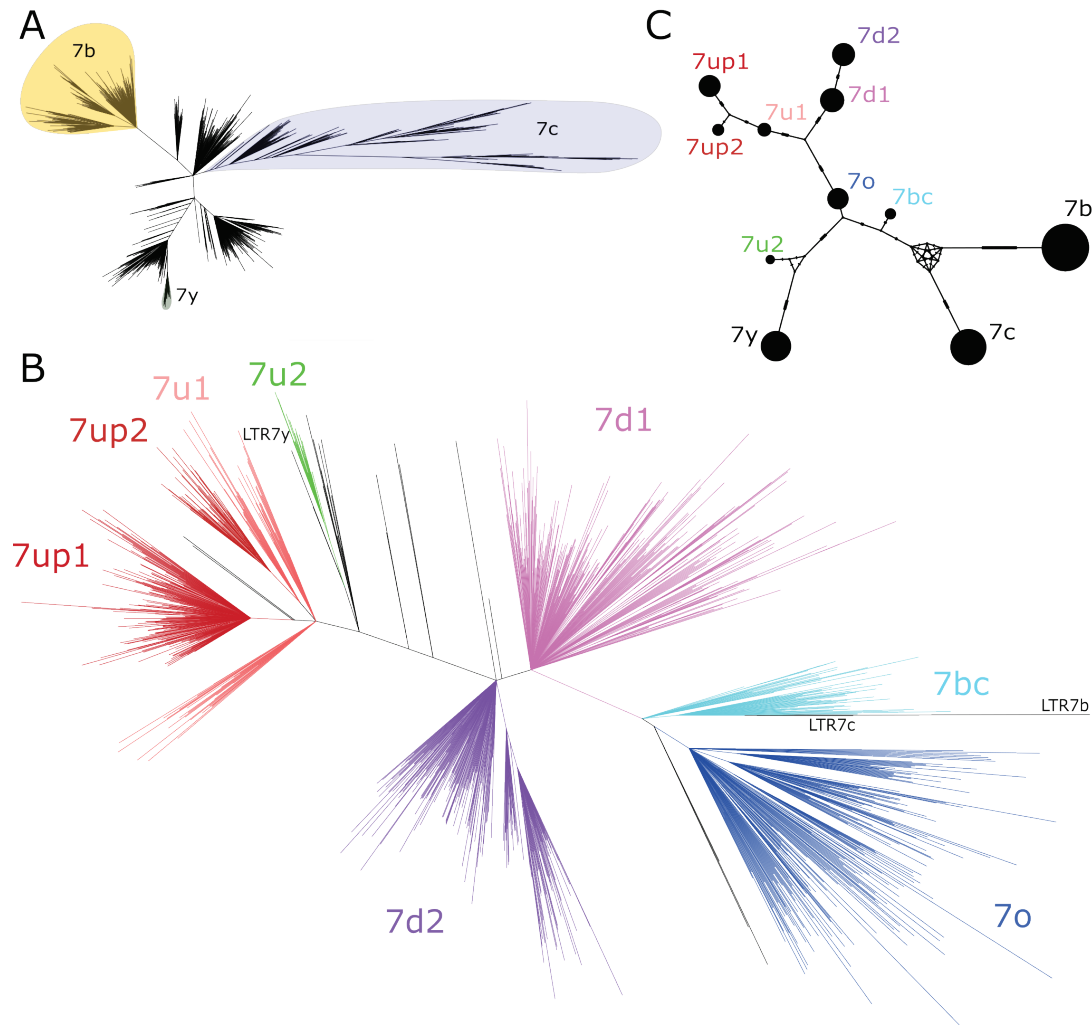


Fig. 1: Phylogenetic analysis of LTR7 sequences. A) Unrooted phylogeny of all solo and 5' LTR7 sequences. All nodes with UFbootstraps >0.95, >10 member insertions, and >1.5 substitutions / 100 bp (~6 base pairs) are grouped and colored (see methods). Previously listed consensus sequences from 7b/c/y were included in the alignment and are shown in black. B) Unrooted phylogeny of all solo and 5' LTR7 subfamilies from 1a, 7b, 7c, and 7y. Colors denote clades consisting of previously annotated 7b, 7c, and 7y with >95% concordance. C) Median joining network analysis of all LTR7 and related majority rule consensus sequences. Ticks indicate the number of SNPs at non-gaps between consensus sequences. The size of circles is proportional to the number of members in each subfamily. Only LTR7 insertions that met filtering requirements (see methods) are included while 7b/c/y counts are from dfam.

133 common ancestor. To approximate the sequence of these ancestral elements we  
134 generated majority-rule consensus sequence for each of the 8 newly defined LTR7  
135 subfamilies (7o, 7bc, 7up, etc.). The consensus sequences were deposited at  
136 [www.dfam.org](http://www.dfam.org).

137 To investigate the evolutionary relationships among the newly defined and previously  
138 known LTR7 subfamilies, we conducted a median-joining network analysis (Leigh and

139 Bryant, 2015) of their consensus sequences (Fig. 1C). The network analysis provides  
140 additional information on the relationships between subfamilies and approximates the  
141 shortest and most parsimonious paths between them (Bandelt et al., 1999; Cordaux et  
142 al., 2004; Posada and Crandall, 2001). The results place 7o in a central position from  
143 which two major lineages are derived. One lineage led to two sub-lineages, formed by  
144 7up1, 7up2, and 7u1 (with 7up1 and 7up2 being most closely related) and by 7d1 and  
145 7d2. The other lineage emanating from 7o rapidly split into two sub-lineages; one gave  
146 rise to 7u2 and then to 7y and the other gave rise to 7bc which is connected to the two  
147 more diverged subfamilies 7b and 7c (Fig. 1C). Together these results indicate that the  
148 LTRs of HERVH elements can be divided into additional subfamilies than those  
149 previously recognized.

150

### 151 **The age of LTR7 subfamilies suggests three major waves of HERVH propagation**

152 The genetic differences between LTR7 subfamilies suggest that they may have been  
153 active at different evolutionary timepoints. To examine this, we used reciprocal *liftover*  
154 analysis to infer the presence/absence of each human LTR7 locus across five other  
155 primate genomes. Insertions shared at orthologous genomic position across a set of  
156 species are deemed to be ancestral to these species and thus can be inferred to be at  
157 least as old as the divergence time of these species (Johnson, 2019).

158 The results of this cross-species analysis indicate that LTR7 subfamilies have been  
159 transpositionally active at different timepoints in the primate lineage (Fig. 3A). The



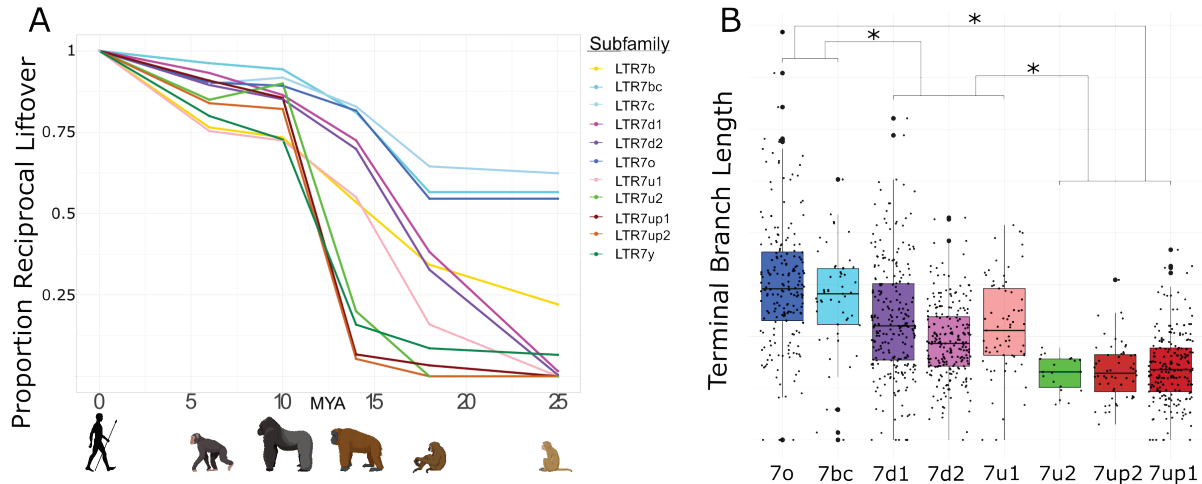


Fig. 2: Age analysis of LTR7 subfamilies. A) Proportion of a given subfamily that have 1:1 orthologous insertions between human and other primate species. LTR7 subfamilies are from trees in Figs. 1a and 2a; 7b/c/y subfamilies are from RepeatMasker annotations. Non-human primates are spaced out on the X axis in accordance with their approximate divergence times to the human lineage. B) Terminal branch lengths of all LTR7 insertions from Fig. 1a. Groups with similar liftover profiles were merged for statistical testing (see methods). Differences with  $\text{padj} < 1e-15$  are denoted with \* (Wilcox rank-sum test with Bonferroni correction).

160 subfamilies 7o, 7bc, and 7c are the oldest since the majority of their insertions are found  
 161 at orthologous position in rhesus macaque, an Old World Monkey (OWM). These three  
 162 subfamilies share similar evolutionary trajectories, with most of their proliferation  
 163 occurring prior to the split of OWM and hominoids, ~25 mya (Fig. 2a). Members of the  
 164 7b subfamily (the most numerous, 637 solo and full-length insertions) appear to be  
 165 overall younger, since only 22% of the human 7b elements could be lifted over to  
 166 rhesus macaque and the vast majority appeared to have inserted between 10 and 20  
 167 mya (Fig. 2A, Figure supplement 1). Only 5 of the 550 elements in the 7d1 and 7d2  
 168 subfamilies could be retrieved in rhesus macaque, but ~30% were shared with gibbon  
 169 and ~75% were shared with orangutan. Thus, these two subfamilies are largely  
 170 hominoid-specific and achieved most of their proliferation prior to the split of African and  
 171 Asian great apes ~14 mya (Fig. 3a). Members of the 7u1 subfamily also emerged in the  
 172 hominoid ancestor, but the majority (55%) of 7u1 elements present in the human  
 173 genome inserted after the split of gibbons in the great ape ancestor, between 14 and 20  
 174 mya. Thus, the 7b, 7d1/2, and 7u1 subfamilies primarily amplified during the same  
 175 evolutionary window, 14 to 20 mya.

176 The 7up1/2, 7y, and 7u2 subfamilies represent the youngest in the human genome, with  
177 most of their proliferation occurring between ~10 and ~14 mya, in the ancestor of  
178 African great apes (Fig. 3A). Based on these results, these subfamilies seem to have  
179 experienced a burst of transposition after the divergence of African and Asian great  
180 apes but before the split of the pan/homo and gorilla lineages. For example, only 14 of  
181 the 208 (6.7%) human 7up1 elements can be retrieved in orangutan, but 178 (85.6%)  
182 can be found in gorilla. These data indicate that the three youngest LTR7 subfamilies  
183 mostly expanded in the ancestor of African great apes (Fig. 2C).

184 As an independent dating method, we used the terminal branch length separating each  
185 insertion from its nearest node in Fig. 1B (Fig. 2B). Here, the terminal branch lengths  
186 are proportional to nucleotide divergence accumulated after insertion and can thus  
187 approximate each insertion's relative age. This method largely corroborated the results  
188 of the *lifter* analysis and revealed three age groups among LTR7 subfamilies  
189 characterized by statistically different mean branch lengths ( $p(\text{adj}) < 1e-15$ ; Wilcoxon rank-  
190 sum test). By contrast, we found no statistical difference between the mean branch  
191 length of the subfamilies within these three age groups, suggesting that they were  
192 concomitantly active. Taken together, our dating analyses distinguish 3 major waves of  
193 HERV propagation: an older wave 25-40 mya involving 7c, 7o, and 7bc elements, an  
194 intermediate wave 9-20 mya involving 7b, 7d1/2 and 7u1, and a most recent wave 4-10  
195 mya implicating primarily 7up1/2, 7u2 and 7y elements.

196

### 197 **Only LTR7up shows robust transcription in human ESC and iPSC**

198 Our data thus far indicate that LTR7 is composed of genetically and evolutionarily  
199 distinct subfamilies. Because a subset of HERVH elements linked to LTR7 were  
200 previously reported to be transcribed in pluripotent stem cells (human ESCs and  
201 iPSCs), we wondered whether this activity was restricted to one or several of the LTR7  
202 subfamilies newly defined herein. To investigate this, we performed a “phyloregulatory”  
203 analysis, where we layered locus-specific regulatory data obtained from publicly  
204 available genome-wide assays in ESCs (mostly from the H1 cell line, see methods) for  
205 each LTR insertion on top of a phylogenetic tree depicting their evolutionary

206 relationship. We called an individual LTR7 insertion as positive for a given feature if  
207 there is overlap between the coordinates of the LTR and that of a peak called for this  
208 mark (see methods). We predicted that if transcriptional activity was an ancestral  
209 property of a given subfamily, evidence of transcription and “activation” marks should be  
210 clustered within the cognate clade. Alternatively, if transcription and activation marks  
211 were to be distributed throughout the tree, it would indicate that LTR7 transcriptional  
212 activity in pluripotent cells was primarily driven by post-insertional changes or context-  
213 specific effects. Differences in the proportion of positive insertions for a given mark  
214 between LTR7 subfamilies were tested using a chi-square test with Bonferroni  
215 correction. Unless otherwise noted, all proportions compared thereafter were  
216 significantly different ( $p_{adj} < 0.05$ ).

217 The results (Fig. 3A) show that HERVH elements inferred to be “highly expressed”  
218 ( $f_{pkm} > 2$ ) based on RNA-seq analysis (Wang et al., 2014) were largely confined to two  
219 closely related subfamilies, 7up1 and 7up2, together referred to as 7up hereafter.  
220 Indeed, we estimated that 33% of 7up elements (88 loci) are highly expressed  
221 according to RNA-seq compared with only 2% of highly expressed elements from all  
222 other subfamilies combined (17 loci). Nascent RNA mapping using GRO-seq data  
223 (Estarás et al., 2015) recapitulated this trend with 22% of 7up loci with visible signal  
224 (Figure supplement 2), compared with only 4% of other LTR7 loci (Fig. 3D, Figure  
225 supplement 2). Half of the loci displaying GRO-seq signal (53/96) also showed evidence  
226 of mature RNA product (supp. file 1). Thus, HERVH transcriptional activity in H1 ESCs  
227 is largely limited to loci driven by 7up sequences.

228 As previously noted from ChIP-seq data (Ohnuki et al., 2014), we found that KLF4  
229 binding is a strong predictor of transcriptional activity: KLF4 ChIP-seq peaks overlap  
230 91% of 7up loci and KLF4 binding is strongly enriched for the 7up subfamilies relative to  
231 other subfamilies (Fig. 3A,B,D). NANOG binding is also enriched for 7up (97.7% of loci  
232 overlap ChIP-seq peaks) but is observed to varying degrees at other LTR7 loci that do  
233 not show evidence of active transcription based on GRO-seq and/or RNA-seq (85% of  
234 7u1 loci, 32% 7d1, 45% 7d2, 13% 7o, 8.7% 7bc, and 0% of 7u2). Other TFs with known  
235 roles in pluripotency are also enriched at 7up loci, such as SOX2 (32% LTR7up, 1-3%

236 all other LTR7), FOXP1(49%, 0-4.3%), and FOXA1(28%, 0-1.4%). In fact, FOXA1 binds  
237 only a single non-7up insertion in our dataset, making it the most exclusive feature of  
238 7up loci among the TFs examined in this analysis. In contrast, OCT4 binds merely 12%  
239 of 7up loci (see supp. file 8 for full statistical analysis of all marks).

240 Congruent with having generally more TF binding and transcriptional activity, 7up loci  
241 also have a propensity to be decorated by H3K4me3, a mark of active promoters (76%  
242 LTR7up vs 19% all others) and the broader activity mark H3K27ac (89% vs 48%) (Fig.  
243 3A,B). By contrast, H3K4me1, a mark typically associated with low POLII loading as  
244 seen at enhancers as opposed to promoters, is spread rather evenly throughout the tree  
245 of LTR7 sequences (26% vs. 18%) (Fig. 2A,B). Thus, promoter marks are primarily  
246 restricted to 7up loci, but a broader range of 7up loci display putative enhancer marks.

247 Taken together, our phyloregulatory analysis suggests that strong promoter activity in  
248 ESCs is restricted to 7up elements.

249

### 250 **Differential activation, rather than repression, explain the differential** 251 **transcriptional activity of LTR7 subfamilies in ESCs**

252 The pattern described above could be explained by two non-mutually exclusive  
253 hypotheses: (i) 7up elements (most likely their progenitor) have acquired unique  
254 sequences (TF binding sites, TFBS) that promote Pol II recruitment and active  
255 transcription, and/or (ii) they somehow escape repressive mechanisms that actively  
256 target the other subfamilies, preventing their transcription. For instance, 7up elements  
257 may lack sequences targeted by transcriptional repressors such as KRAB-Zinc Finger  
258 proteins (KZFP) that silence the other subfamilies in ESCs. KZFP are well-known for  
259 binding TEs in a subfamily-specific manner where they nucleate inheritable epigenetic  
260 silencing (Ecco et al., 2017; Jacobs et al., 2014; Wolf et al., 2020; Yang et al., 2017)  
261 and several KZFPs are known to be capable of binding LTR7 loci (Imbeault et al.,  
262 2017). To examine whether KZFPs may differentially bind to LTR7 subfamilies, we  
263 analyzed the loading of the corepressor KAP1 and the repressive histone mark

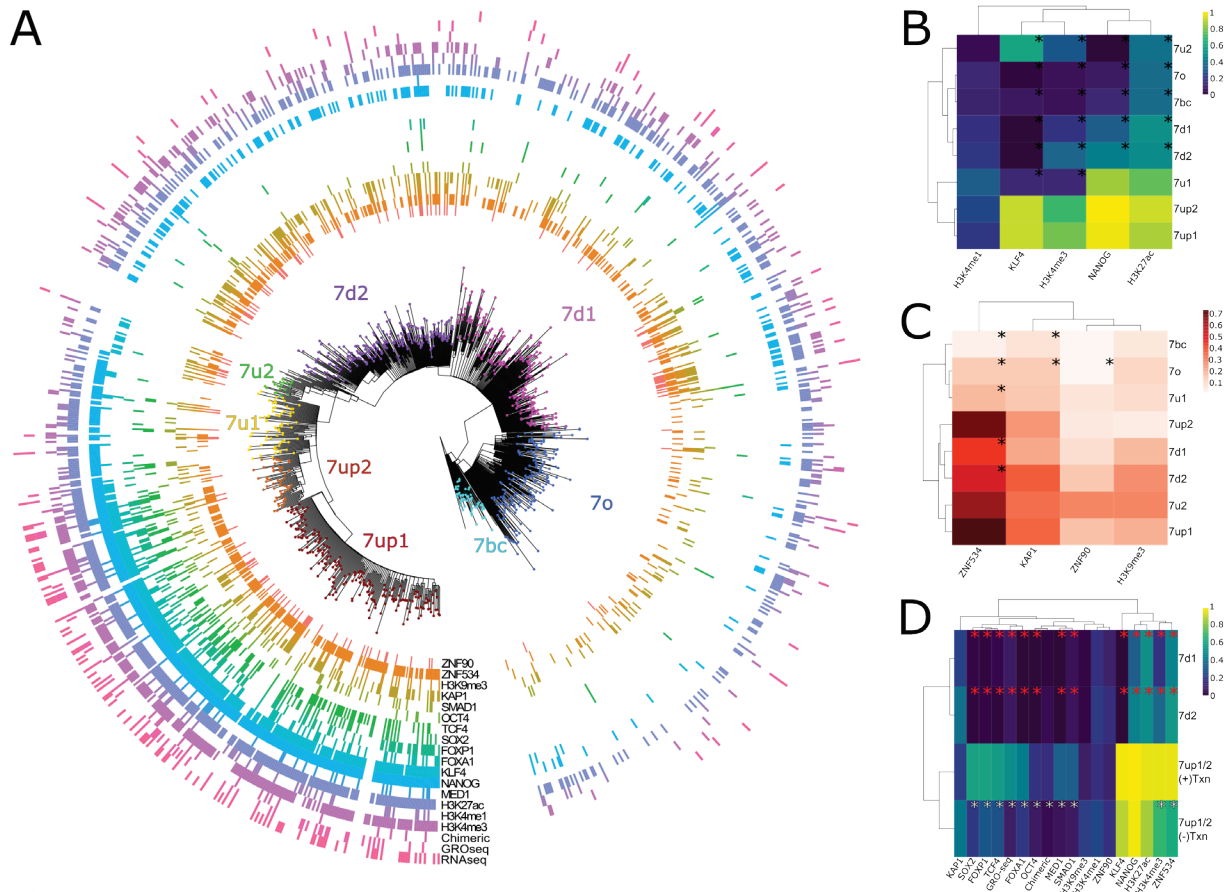


Fig. 3: Phyloregulatory analysis of LTR7. A) “Phyloregulatory” map of LTR7. The phylogenetic analysis to derive the circular tree is the same as for the tree in Fig. 1A but rooted on the 7b consensus. Subfamilies defined in Fig. 1 are denoted with dotted colored tips. Positive regulatory calls for each insertion are shown as tick marks of different colors and no tick mark indicates a negative call. All marks are derived from ESC except for ZNF90 and ZNF534, which are derived from ChIP-exo data after overexpression of these factors in HEK293 cells (see methods) B) Heatmap of major activation and repression profiles. Proportions indicate the proportion of each group positive for a given characteristic. Trees group LTR7 subfamilies on regulatory signature, not sequence similarity. Asterisks denote statistical differences between given group and 7up1 ( $p_{adj} > 0.05$  Wilcoxon rank-sum with Bonferroni correction). C) Heatmap done in similar fashion to Fig. 3B but for repression marks. D) Heatmap of transcribed ( $>2$  fpkm) and untranscribed ( $<2$  fpkm) 7up1/2 and all 7d1/2. Red asterisks denote statistical differences between 7d1/2 and 7up1 ( $p_{adj} < 0.05$  chi-square Bonferroni correction). White asterisks denote differences between transcribed and untranscribed LTR7up.

264 H3K9me3 typically deposited through the KZFP/KAP1 complex, across the LTR7  
 265 phylogeny using ChIP-seq data previously generated for ESCs (Imbeault et al., 2017;  
 266 Theunissen et al., 2016). We found that KAP1 and H3K9me3 loading were neither  
 267 enriched nor depleted for 7up elements relative to other subfamilies (Fig. 3A,C). Overall,  
 268 there were no significant differences in the level of H3K9me3 marking across  
 269 subfamilies and the only difference in KAP1 binding was a slight but significant

270 depletion for 7bc and 7o compared to all other subfamilies including 7up (14% vs. 35% -  
271  $\text{padj} < 0.05$  chi-square Bonferroni correction). Furthermore, KAP1 and H3K9me3 loading  
272 were found in similar proportions in expressed and unexpressed 7up elements ( $\text{padj} >$   
273 0.05) (Fig. 2C). This was also the case for CpG methylation, whose presence was not  
274 differential between subfamilies ( $\text{padj} > 0.05$  Wilcoxon rank-sum with Bonferroni correction)  
275 (Figure supplement 2). Thus, KAP1 binding and repressive marks at LTR7 in ESCs  
276 poorly correlate with their transcriptional activity and differential repression is unlikely to  
277 explain the differential promoter activity of LTR7 subfamilies in ESCs.

278 We also examined the binding profile of ZNF534 and ZNF90, two KZFPs previously  
279 reported to be enriched for binding LTR7 elements using CHIP-exo data in human  
280 embryonic kidney 293 cells (Imbeault et al., 2017), in order to examine whether they  
281 bind a particular subset of elements in our LTR7 phylogeny. We found that while ZNF90  
282 bound all LTR7 subfamilies to a similar extent, ZNF534 preferentially bound members of  
283 the 7up subfamily (72% of LTR7up vs. 34-53% of non-LTR7up). However, ZNF534  
284 binding in 293 cells did not correlate with transcriptional activity of 7up elements in  
285 ESCs nor with KAP1 binding or H3K9me3 deposition in these cells (Fig. 3A,D). In other  
286 words, there was no significant enrichment for ZNF534 binding within untranscribed 7up  
287 elements nor depletion within the 7up elements we inferred to be highly transcribed in  
288 ESCs. These observations could simply reflect the fact that ZNF534 itself is not highly  
289 expressed in ESCs (Figure supplement 3) and do not preclude that ZNF534 represses  
290 7up in other cellular contexts or cell types. Collectively these data suggest that  
291 differential LTR binding of KZFP/KAP1 across subfamilies cannot readily explain their  
292 differential regulatory activities in ESCs. Thus, differential activation is the most likely  
293 driver for the promoter activity of 7up elements in ESCs.

294 To determine which factors are associated and potentially determinant for 7up promoter  
295 activity, we compared the set of “highly expressed” 7up loci to 7up loci which are  
296 apparently poorly expressed, using 7d1/d2 as outgroups (Fig. 3D). While known  
297 regulators of LTR7 transcription, KLF4 and NANOG, are enriched for binding to 7up  
298 elements, their occupancy alone cannot distinguish transcribed from untranscribed 7up  
299 loci (Fig. 3D). Thus, other factors must contribute to the transcriptional activation of 7up



300 elements. Our analysis of pluripotent transcriptional activators SOX2, FOXA1, FOXP1,  
301 OCT4, TCF4, and SMAD1 (Boyer et al., 2005; Chambers and Smith, 2004; Niwa, 2007)  
302 binding profiles show that all of these TFs are enriched in robustly transcribed 7up loci  
303 compared to non-transcribed loci (Fig. 3D). Intriguingly, when overexpressed in HEK293  
304 cells, the potential KZFP repressor ZNF534 preferably binds ESC-transcribed 7up over  
305 untranscribed 7up, suggesting that ZNF534 may suppress transcription-competent 7up  
306 in cellular contexts where this factor is expressed.

307 Together these data suggest that differential repression cannot explain the differential  
308 promoter activity of LTR7 subfamilies in ESCs but rather that highly expressed LTR7up  
309 loci are preferentially bound by a cocktail of transcriptional activators that are less  
310 prevalent on poorly-expressed loci.

311

### 312 **Inter-element recombination and intra-element duplication drove LTR7 sequence** 313 **evolution**

314 The data presented above suggest that the transcriptional activity of 7up in ESCs  
315 emerged from the gain of a unique combination of TFBS. To identify sequences unique  
316 to 7up relative to its closely related subfamilies, we aligned the consensus sequences of  
317 the newly defined LTR7 subfamilies and those of 7b/c/y consensus sequences. This  
318 multiple sequence alignment revealed blocks of sequences that tend to be highly  
319 conserved across subfamilies, only diverging by a few SNPs, while other regions  
320 showed insertion/deletion (indel) segments specific to one or a few subfamilies (Fig.  
321 4A). These indels resulted in substantial gain and loss of DNA between closely related  
322 subfamilies, with the longest consensus (7y) having a length of 472-bp and the shortest  
323 (7o) a mere 365-bp. These observations suggest that segmental rearrangements have  
324 played an important role in the evolution of LTR7 sequences.

325 Upon closer scrutiny, we noticed that the indels characterizing some of the subfamilies  
326 were at odds with the evolutionary relationship of the subfamilies defined by overall  
327 phylogenetic and network analyses. This was particularly obvious in segments we

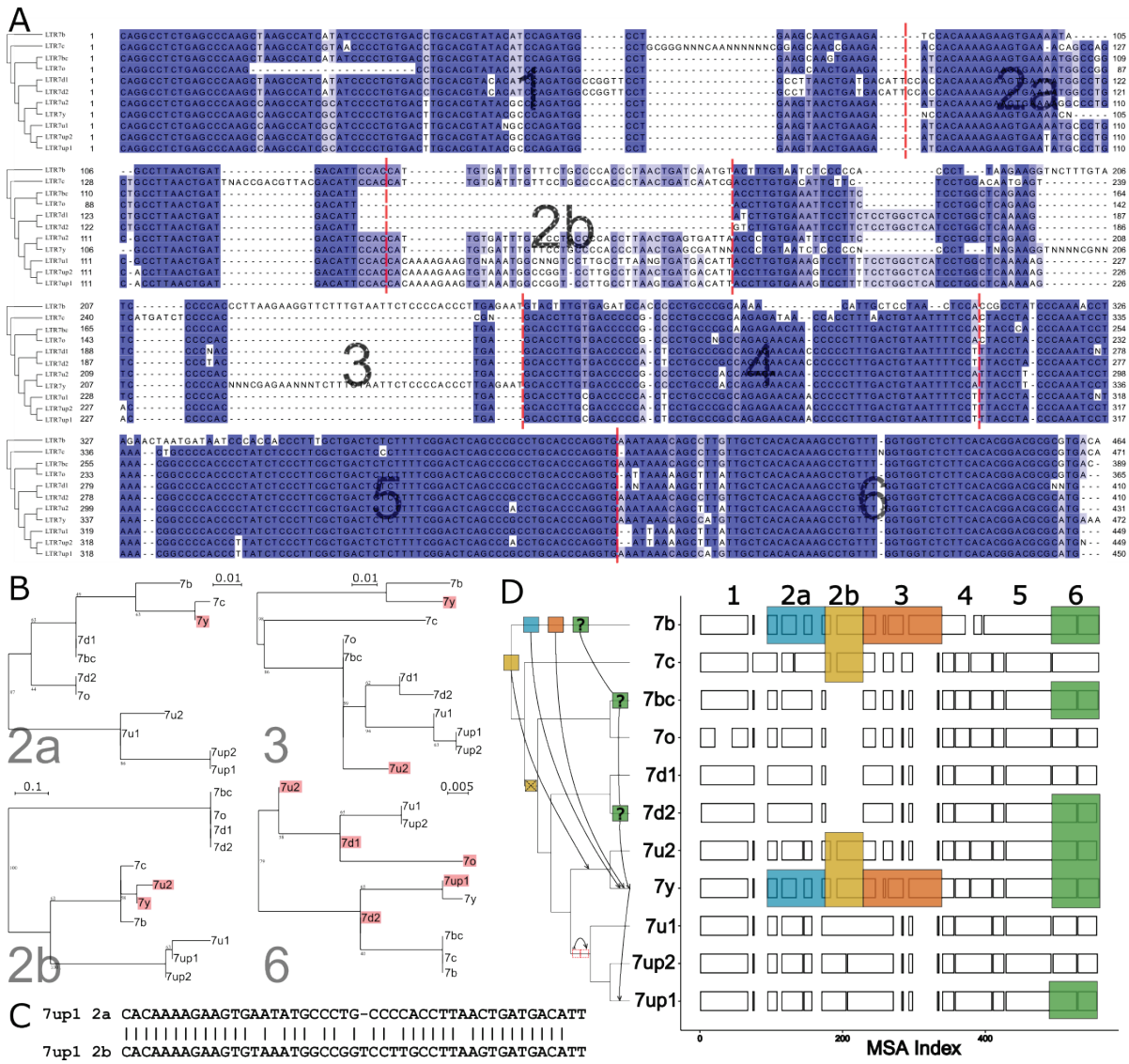


Fig. 4: Modular block evolution of LTR7 subfamilies. A) A multiple sequence alignment of LTR7 subfamily consensus sequences. The phylogenetic topology from Figure 1 is shown on the left. The MSA is broken down into sequence blocks (red lines) with differential patterns of relationships. B) Parsimony trees from Fig. 4a sequence blocks. Subfamilies whose blocks do not match the overall phylogeny are highlighted in red. Bootstrap values >0 are shown. C) Blastn alignment of LTR7up1 block 2a and 2b. D) A multiple sequence alignment of majority-rule consensus sequences from each LTR7 subfamily detailing shared structure. Blocks show aligned sequence; gaps represent absent sequence. Colored sections identify putative phylogeny-breaking events. Recombination events whose directionality can be inferred (via aging) are shown with blocks and arrows on the cladogram. Recombination events with multiple possible routes are denoted with "?". The deletion of 2b is denoted on the cladogram with a red "X"; the duplication of 2a is denoted with 2 red rectangles.

328 termed block 2b (where 7y and 7u2 share a large insertion with 7b and 7c) and block 3  
 329 (where 7y and 7b share a large insertion). This led us to carefully examine the multiple  
 330 sequence alignment of the LTR7 consensus sequences to identify indels with different



331 patterns of inter-subfamily relationships. Based on this analysis, we defined seven  
332 sequence blocks shared by a different subset of subfamilies, pointing at relationships  
333 that were at odds with the overall phylogeny of the LTR7 subfamilies (Fig. 4A-B). These  
334 observations suggested that some of the blocks have been exchanged between LTR7  
335 subfamilies through recombination events.

336 To systematically test if recombination events between elements drove the evolution of  
337 LTR7 subfamilies, we generated parsimony trees for each block of consensus  
338 sequences and looked for incongruences with the overall consensus phylogeny. We  
339 found a minimum of 6 instances of clades supported in the block parsimony trees that  
340 were incongruent with those supported by the overall phylogeny (Fig. 4B,D).

341 We also found some blocks evolved via tandem duplication. Notably, block 2b was  
342 absent from 7d1/2 and 7bc/o but present in all other subfamilies. However, block 2b  
343 from 7b, 7c, 7u2, and 7y aligned poorly with block 2b from 7up and 7u1. Instead, block  
344 2b from 7up/u1 2b was closely related (~81% nucleotide similarity) to block 2a from the  
345 same subfamilies (Fig. 4D), suggestive that it arose via tandem duplication in the  
346 common ancestor of these subfamilies. To further clarify the evolutionary history of the  
347 2a-2b duplication, we aligned all 2a and 2b blocks from all subfamilies and generated a  
348 parsimony tree (Figure supplement 4). This analysis indicated that the 2b block from  
349 7up/u1 most closely resembles the 2a block from 7d.

350 The results above suggest that the evolution of HERVH was characterized by extensive  
351 diversification of LTR sequences through a mixture of point mutations, indels, and  
352 recombination events.

353

### 354 **HERVH subfamilies show distinct expression profiles in the preimplantation** 355 **embryo**

356 We hypothesized that the mosaic pattern of LTR sequence evolution described above  
357 gave rise to TFBS combinations unique to each family that drove shifts in HERVH  
358 expression during early embryogenesis. To test this, we aimed to reanalyze the  
359 expression profiles of newly defined LTR7 subfamilies during early human

360 embryogenesis and correlate these patterns with the acquisition of embryonic TF  
 361 binding motifs within each of the subfamilies.

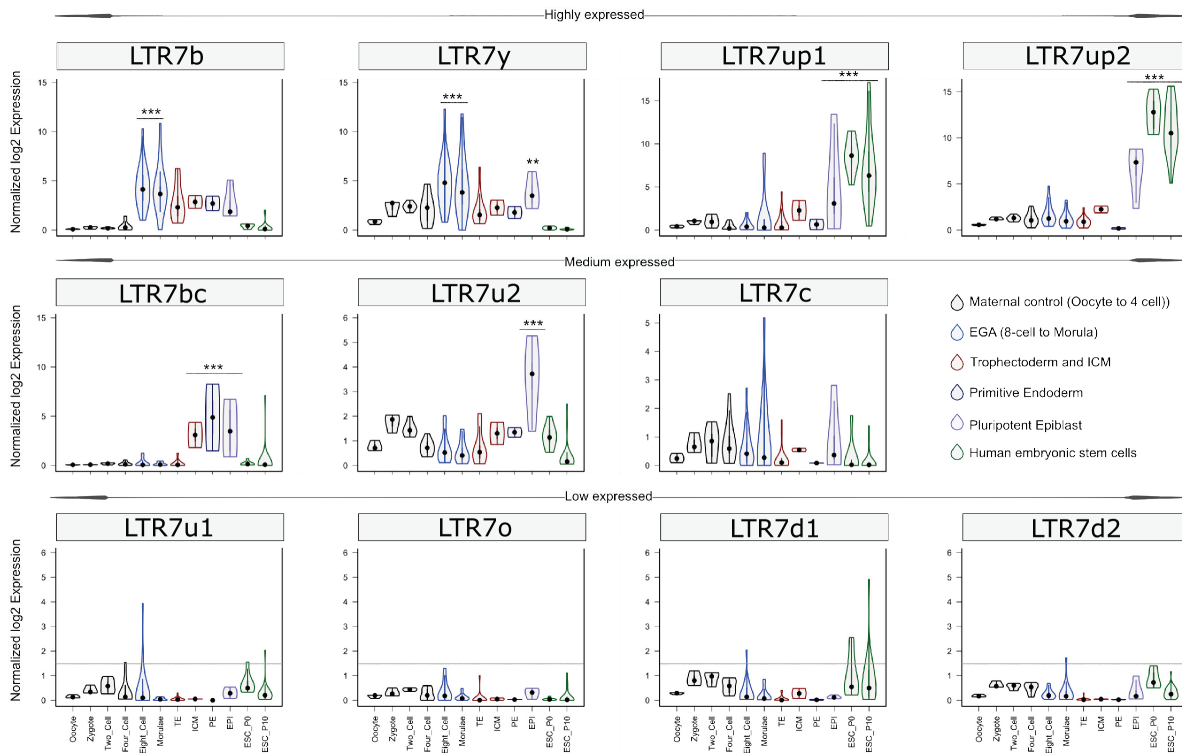


Fig. 5: Expression profile of LTR7 subfamilies in human preimplantation embryonic lineages and ESCs. The solid dots and lines encompassing the violins represent the median and quartiles of single cellular RNA expression. The color scheme is based on embryonic stages, defined as maternal control of early embryos (Oocytes, Zygote, 2-cell and 4-cell stage), EGA (8-cell and Morula), inner cell mass (ICM), trophoctoderm (TE), epiblast (EPI) and primitive endoderm (PE) from the blastocyst, and ESCs at passages 0 and 10.

362 To perform this analysis, we first reannotated the hg38 reference genome assembly  
 363 using Repeatmasker with a custom library consisting of the consensus sequences for  
 364 the 8 newly defined LTR7 subfamilies plus newly generated consensus sequences for  
 365 7b, 7c, and 7y subfamilies redefined from the phylogenetic analysis presented in Fig. 1B  
 366 (Figure supplement 5) (see methods). Our newly generated Repeatmasker annotations  
 367 (supp. file 2) did not drastically differ from previous annotations of LTR7 and 7c, where  
 368 90% and 86% of insertions, respectively, were concordant with the old Repeatmasker  
 369 annotations (though LTR7 insertions were now assigned to one of the 8 newly defined  
 370 subfamilies). 7y and 7b annotations, however, shifted significantly. Only 33% of  
 371 previously annotated 7y reannotated concordantly with 53% now being annotated as  
 372 7u2 and only 52% of 7b reannotated concordantly, with 22% now annotated as 7y.

373 These shifts can be largely explained by the fact that 7u2 and 7y are closely related  
374 (Fig. 1A-C) and 7y and 7b share a great deal of sequence through recombination  
375 events (Fig. 4B-C).

376 Next we used the newly generated Repeatmasker annotations to examine the RNA  
377 expression profiles of the different LTR7 subfamilies using scRNA-seq data from human  
378 pre-implantation embryos and RNA-seq data from human ESCs (Blakeley et al., 2015;  
379 Tang et al., 2010) (see methods).

380 As expected, we found that the 7up subfamilies were highly expressed in the pluripotent  
381 epiblast and in ESCs (Fig. 5). 7up expression was highly specific to these pluripotent  
382 cell types, with little to no transcription at earlier developmental time points. As  
383 previously observed (Göke et al., 2015), the 7b subfamily exhibited expression at the 8-  
384 cell and morula stages, coinciding with EGA (Fig. 5). Another remarkable expression  
385 pattern was that of 7u2 which was restricted to the pluripotent epiblast (Fig. 5).

386 Interestingly, the 7y subfamily combined the expression of 7b and 7u2 (8-cell and  
387 morula plus epiblast), perhaps reflecting the acquisition of sequence blocks from both  
388 subfamilies (Fig. 4B-C). Despite very similar sequence and age (Fig. 1, Fig. 2, Fig. 4A),  
389 7bc and 7o elements show stark contrast in their expression profiles. 7o elements show  
390 no significant transcription at any time point in early development, while 7bc elements  
391 display RNA expression throughout the blastocyst, including trophectoderm and inner  
392 cell mass, primitive endoderm, and pluripotent epiblast (Fig. 5). Previous expression  
393 analysis of the oldest LTR7 subfamily, 7c, did not find robust stage-specific expression  
394 (Göke et al., 2015). Our analysis revealed that some 7c elements display moderate  
395 RNA expression at various developmental stages (Fig. 5). This pattern may reflect the  
396 relatively high level of sequence heterogeneity within this subfamily (Fig. 1).

397 In summary, our analysis indicates that LTR7 subfamilies have distinct but partially  
398 overlapping expression profiles during human early embryonic development that appear  
399 to mirror their complex history of sequence diversification.

400

401 **A predicted SOX2/3 motif unique to 7up is required for transcriptional activity in**  
402 **pluripotent stem cells**

403 We hypothesized that differences in embryonic transcription among LTR7 subfamilies  
404 were driven by the gain and loss of TF binding motifs, and that one or more of these  
405 mutations led to 7up's pluripotent-specific transcription. To find TF motifs enriched  
406 within each LTR7 subfamily relative to the others, we performed an unbiased motif  
407 enrichment analysis using the program HOMER to calculate enrichment scores of  
408 known TF motifs within each segmental block defined in Fig. 4A in a pairwise  
409 comparison of each subfamily against each of the other subfamilies (see methods). The  
410 results yielded a slew of TF motifs enriched for each subfamily relative to the others  
411 (see Fig. 6A for 7up1 and enrichment for all HERVH subfamilies in supp. files 3,4).  
412 These results suggested that each LTR7 subfamily possesses a unique repertoire of TF  
413 binding motifs, which could explain their differential expression during embryonic  
414 development.

415 Next, we sought to pinpoint mutational events responsible for the gain of TF motifs  
416 responsible for the unique expression of 7up in ESC. The single most striking motif  
417 distinguishing the 7up clade from the others was a SOX2/3 motif which coincided with  
418 an 8-bp insertion in block 2b (Fig. 6A,B). Note this motif (and insertion) was also present  
419 in 7u1, the closest relative to 7up (Fig. 4C), but absent in all other subfamilies (Fig. 6B).

420 We hypothesized that the 8-bp insertion provided a binding motif for SOX2 and/or SOX3  
421 contributing to 7up promoter activity in ESCs. Indeed, SOX2 and SOX3 bind a highly  
422 similar motif (Bergsland et al., 2011; Heinz et al., 2010), activate an overlapping set of  
423 genes and play a redundant function in pluripotency (Corsinotti et al., 2017; Niwa et al.,  
424 2016; Wang et al., 2012). In addition, we observed that both SOX2 and SOX3 are  
425 expressed in human ESCs but SOX3 was more highly and more specifically expressed  
426 in ESCs (Figure supplement 6A,C). While SOX3 binding has not been profiled in human  
427 ESCs, ChIP-seq data available for SOX2 indicated that it binds preferentially 7up in a  
428 region coinciding with the 8-bp motif (Fig. 6B). Together these observations suggest  
429 that 7up promoter activity in ESCs might be conferred in part by the gain of a SOX2/3  
430 motif in block 2b.

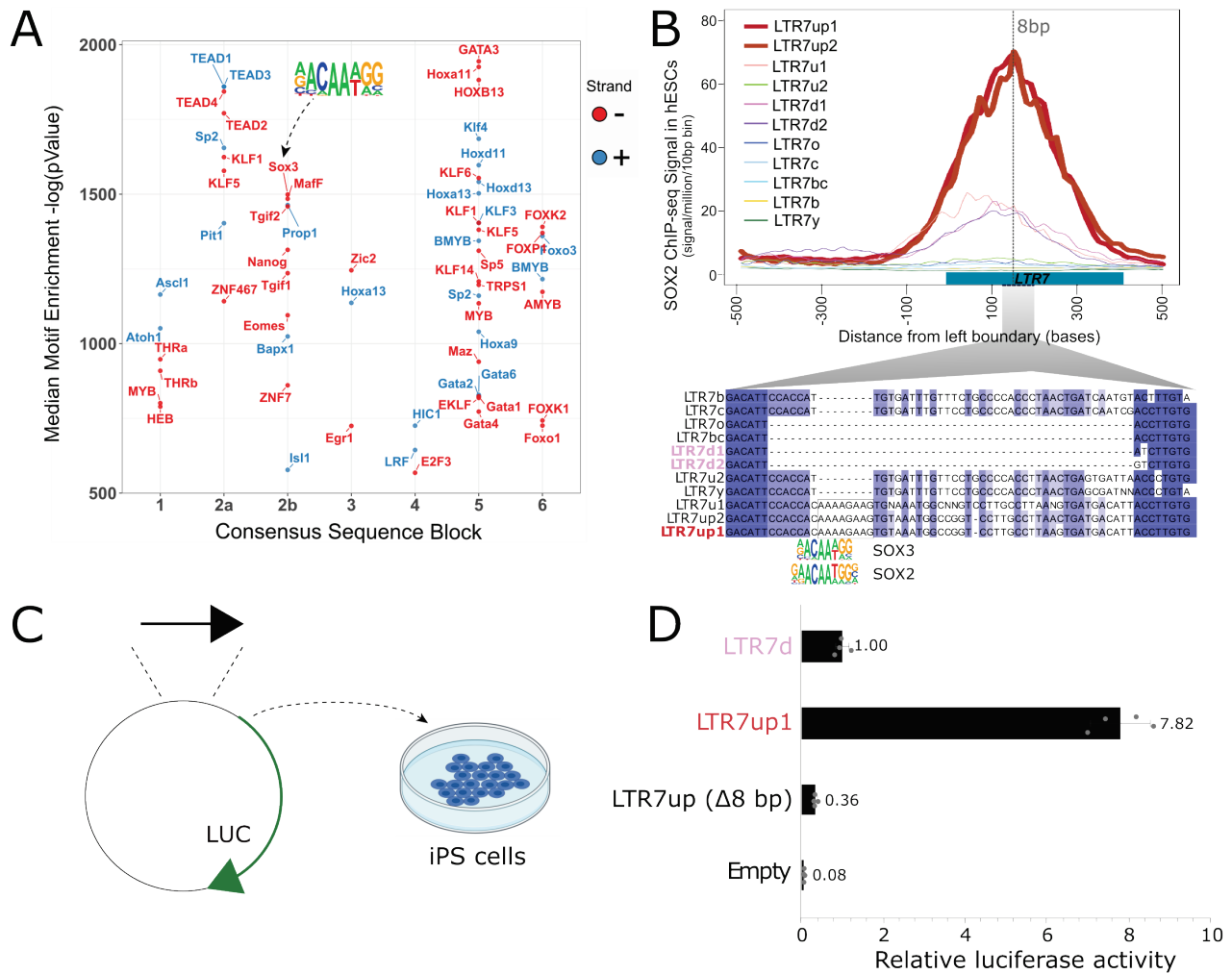


Fig. 6: An 8-bp insertion, SOX2/3 binding site necessary for LTR7up transcription. A) (log) p-values >500 for HOMER motifs enriched in 7up1 insertion's sequence blocks vs the same blocks from other insertions from other HERVH subfamilies are shown. B) Line plots show SOX2 ChIP-seq signal at LTR7 subfamily loci in human ESCs. Signal from genomic loci was compiled relative to position 0. The 7up/u1 8bp insertion position is shown with a dotted line. Region 2b harboring SOX2/3 TFBS is detailed below. C) Scheme of DNA fragments cloned into pGL3-basic vector driving luciferase gene expression (LUC) with identified SOX2/3 motifs. 3 constructs were analyzed: Entire LTR7up (7up1), 7d1/2 consensus sequence (approximate ancestral sequence for all LTR7d) and LTR7up with 8 nucleotides deleted (LTR7up (Δ8bp - AAAAGAAG)) (see panel B). D) Normalized relative luciferase activity of tested fragments compared to LTR7 down; n = 4 measurements; bars, means across replicates; error bars, standard deviation of the mean, dots, individual replicates.

431 To experimentally test this prediction, we used a luciferase reporter to assay promoter  
 432 activity of three different LTR7 sequences in iPSCs (see methods). The first consisted  
 433 of the full-length 7d consensus sequence (predicted to be inactive in iPSCs), the second  
 434 contained the full-length 7up1 consensus (predicted to be active) and the third used the  
 435 same 7up1 consensus sequence but lacking the 8-bp motif unique to 7up1/2 and 7u1  
 436 elements overlapping the SOX2/3 motif (Fig. 6B,C). The results of the assays revealed

437 that the 7d construct exhibited, as predicted, only weak promoter activity in iPSC  
438 compared to the empty vector (Fig. 6D), while the 7up1 construct had much stronger  
439 promoter activity, driving on average 7.8-fold more luciferase expression than 7d and  
440 100-fold more than the empty vector (Fig. 6D). Strikingly, the promoter activity was  
441 essentially abolished in the 7up1 construct lacking the 8-bp motif, which drove minimal  
442 luciferase expression (on average, 3-fold less than LTR7d and 20-fold less than the  
443 intact LTR7up sequence). These results demonstrate that the 8-bp motif in 7up1 is  
444 necessary for robust promoter activity in iPSCs, likely by providing a SOX2/3 binding  
445 site essential for this activity.

## 446 **Discussion**

447 The HERVH family has been the subject of intense investigation for its transcriptional  
448 and regulatory activities in human pluripotent stem cells. These studies often have  
449 treated the entire family as one homogenous, monophyletic entity and it has remained  
450 generally unclear which loci are transcribed and potentially important for pluripotency.  
451 This is in part because HERVH/LTR7 is an abundant and young family which poses  
452 technical challenges to interrogate the activity of individual loci and design experiments  
453 targeting specific members of the family (Chuong et al., 2017; Lanciano and Cristofari,  
454 2020). Here, we applied a ‘phyloregulatory’ approach that integrates regulatory  
455 genomics data to a phylogenetic analysis of LTR7 sequences to reveal several new  
456 insights into the origin, evolution, and transcription of HERVH elements. In brief, our  
457 results show that: (i) LTR7 is a polyphyletic group composed of at least eight  
458 monophyletic subfamilies; (ii) these subfamilies have distinct evolutionary histories and  
459 transcriptional profiles in human embryos and a single and relatively small subgroup  
460 (~264 loci), LTR7up, exhibits robust promoter activity in ESC; (iii) LTR7 evolution is  
461 characterized by the gain, loss, and exchange of cis-regulatory modules likely  
462 underlying their transcriptional partitioning during early embryonic development.

463

## 464 **Phyloregulatory analysis of LTR7 disentangles the cis-regulatory evolution of** 465 **HERVH**

466 Previous studies have treated LTR7 *sensu stricto* insertions as equivalent  
467 representatives of their subfamilies (Bao et al., 2015; Gemmell et al., 2019; Göke et al.,  
468 2015; Izsvák et al., 2016; Storer et al., 2021; Wang et al., 2014; Zhang et al., 2019).  
469 While some of these studies were able to detect differential transcriptional partitioning  
470 between LTR7, LTR7y, and LTR7b (Göke et al., 2015), the amalgamating of LTR7 loci  
471 limited the ability to detect transcriptional variations among LTR7 and to identify key  
472 sequence differences responsible for divergent transcription patterns. Our granular  
473 parsing of LTR7 elements and their phyloregulatory profiling has revealed striking  
474 genetic, regulatory, and evolutionary differences amongst these sequences.



475 Importantly, a phylogeny based on the coding sequence (RVT domain) of HERVH  
476 provided less granularity to separate the subfamilies than the LTR sequences (Figure  
477 supplement 7). The classification of new subfamilies within LTR7 enabled us to discover  
478 that they have distinct expression profiles during early embryonic development (Fig. 5)  
479 that were previously obscured by their aggregation into a single group of elements. For  
480 example, the 7u2 subfamily is, to our knowledge, the first subfamily of human TEs  
481 reported to have preimplantation expression exclusively in the epiblast.

482 It has been observed for some time that only a small subset of HERVH elements are  
483 expressed in ESCs (Gemmell et al., 2019; Göke et al., 2015; Ohnuki et al., 2014;  
484 Santoni et al., 2012; Schön et al., 2001; Wang et al., 2014; Zhang et al., 2019). Some  
485 have attributed this property to variation in the internal region of HERVH, context-  
486 dependent effects (local chromatin or cis-regulatory environment) and/or age (Gemmell  
487 et al., 2019; Zhang et al., 2019). Our results provide an additional, perhaps simpler  
488 explanation: we found that HERVH elements expressed in ESCs are almost exclusively  
489 driven by two closely related subfamilies of LTR7 (7up) that emerged most recently in  
490 hominoid evolution. We identified one 8-bp sequence motif overlaps a predicted  
491 SOX2/3 binding site unique to 7up that is required for promoter activity in pluripotent  
492 stem cells. These results highlight that the primary sequence of the LTR plays an  
493 important role in differentiating and diversifying HERVH expression during human  
494 embryonic development.

495 The phyloregulatory approach outlined in this study could be applied to illuminate the  
496 regulatory activities of LTR elements in other cellular contexts. In addition to  
497 embryogenesis, subsets of LTR7 and LTR7y elements are known to be upregulated in  
498 oncogenic states (Babaian and Mager, 2016; Glinsky, 2015; Kong et al., 2019; Yu et al.,  
499 2013). It would be interesting to explore whether these activities can be linked to the  
500 gain of specific TFBS using the new LTR7 annotations and regulatory information  
501 presented herein. Other human LTR families, such as MER41, LTR12C, or LTR13 have  
502 been previously identified as enriched for particular TF binding and cis-regulatory  
503 activities in specific cellular contexts (Chuong et al., 2016; Deniz et al., 2020; Ito et al.,  
504 2017; Krönung et al., 2016; Sundaram et al., 2014). In each case, TF binding



505 enrichment was driven by a relatively small subset of loci within each family. We  
506 suspect that some of the intrafamilial differences in TF binding and cis-regulatory  
507 activity may be caused by unrecognized subfamily structure and subfamily-specific  
508 combinations of TFBS, much like we observe for LTR7.

509

## 510 **Recombination as a driver of LTR cis-regulatory evolution**

511 Recombination is a common and important force in the evolution of exogenous RNA  
512 viruses (Jetzt et al., 2000; Pérez-Losada et al., 2015; Simon-Loriere and Holmes, 2011)  
513 and endogenous retroviruses (Vargiu et al., 2016). Traditional models of recombination  
514 describe recombination occurring due to template switching during reverse transcription,  
515 a process that requires the co-packaging of RNA genomes, a feature of retroviruses  
516 and some retrotransposons (Lai, 1992; Matsuda and Garfinkel, 2009). Previous studies  
517 proposed that the HERVH family had undergone inter-element recombination events of  
518 both its coding genes (Mager and Freeman, 1987; Vargiu et al., 2016) and LTR  
519 (Goodchild et al., 1993). Specifically, it was inferred that recombination event between  
520 Type I LTR (i.e., LTR7) and Type II LTR (LTR7b) led to the emergence of Type Ia  
521 (LTR7y).

522 Our findings of extensive sequence block exchange between 7y and 7b (Fig. 4D) are  
523 consistent with these inferences. Furthermore, our division of HERVH into at least 11  
524 subfamilies, rather than the original trio (Type I, II, Ia), and systematic analysis of  
525 recombination events (Fig. 4) suggest that recombination has occurred between  
526 multiple lineages of elements and has been a pervasive force underlying LTR  
527 diversification. We identified a minimum of six recombination events spanning 20 million  
528 years of primate evolution (see Fig. 4D and summary model in Fig. 7). The coincidence  
529 of recombination events with changes in expression profiles (Fig. 7) suggests that these  
530 events were instrumental to the diversification of HERVH embryonic expression. The  
531 hybrid origin and subsequent burst of amplification of LTR7 subfamilies (Fig. 1,2)  
532 suggest they expanded rapidly after shifting their transcriptional profiles. The  
533 coincidence of niche colonization with a burst in transposition leads us to speculate that  
534 these shifts in expression were foundational to the formation and successful expansion

535 of new HERVH subfamilies. It would be interesting to explore whether inter-element  
 536 recombination has also contributed to the evolution of other LTR subfamilies and the  
 537 diversification of their expression patterns.

538 Previous work has highlighted the role of TEs, and LTRs in particular, in donating built-  
 539 in cis-regulatory sequences promoting the evolutionary rewiring of mammalian  
 540 transcriptional networks (Chuong et al., 2017; Feschotte, 2008; Hermant and Torres-  
 541 Padilla, 2021; Jacques et al., 2013; Rebollo et al., 2012; Sundaram and Wysocka, 2020;  
 542 Thompson et al., 2016). We show that recombination provides another layer to this  
 543 idea, where combinations of TFBS can be mixed-and-matched, then mobilized and  
 544 propagated, further accelerating the diversification of these regulatory DNA elements.  
 545 As HERVH expanded and diversified, its newly evolved cis-regulatory modules became  
 546 confined to specific host lineages (Fig. 2). Thus, it is possible that the formation of new

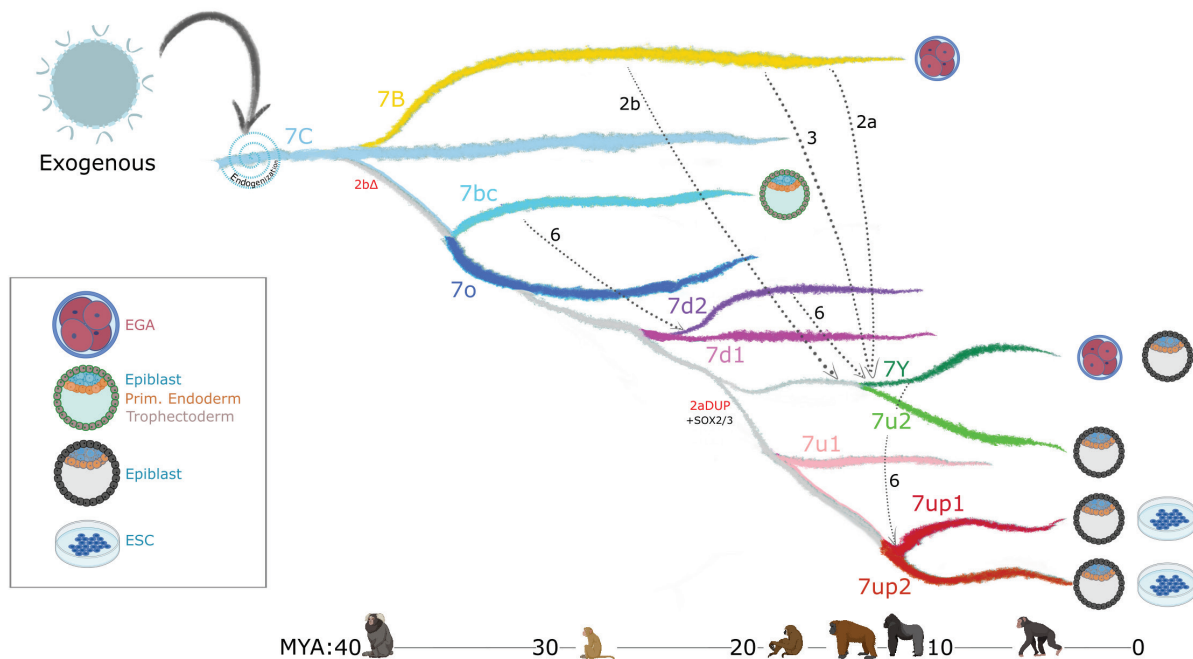


Fig. 7: Model of LTR7 subfamily evolution. Estimated LTR7 subfamily transpositional activity in mya are listed with corresponding approximate primate divergence times (bottom). The positioning and duration of transpositional activity are based on analysis from Fig. 3b. The grey connections between subfamilies indicate average tree topology which is driven by overall pairwise sequence similarity. Dashed lines indicate likely recombination events which led to the founding of new subfamilies. Stage-specific expression profiles from Fig. 5a are detailed to the right of each corresponding branch.

547 LTR via recombination and their subsequent amplification catalyzed cis-regulatory  
548 divergence across primate species.

549

550 **LTR evolution enabled HERVH's colonization of different niches in the human**  
551 **embryo**

552 Our evolutionary analysis reveals that multiple HERVH subfamilies were  
553 transpositionally active in parallel during the past ~25 my of primate evolution (Fig. 2,7).  
554 This is in stark contrast to the pattern of LINE1 evolution in primates, which is  
555 characterized by a single subfamily being predominantly active at any given time (Khan  
556 et al., 2006). We hypothesize that the ability of HERVH to colonize multiple cellular  
557 niches underlie this difference. Indeed, we observe that concurrently active HERVH  
558 subfamilies are transcribed at different developmental stages, such as 7up and 7u2  
559 being transcribed in the pluripotent epiblast at the same time that 7y and the youngest  
560 7b were transcribed at the 8 cell and morula stages (Fig. 7). We posit that this  
561 partitioning allowed multiple HERVH subfamilies to amplify in parallel without causing  
562 overt genome instability and cell death during embryonic development.

563 Niche diversification may have also enabled HERVH to evade cell-type-specific  
564 repression by host-encoded factors such as KZFPs. KZFPs are thought to emerge and  
565 adapt during evolution to silence specific TE subfamilies in a cell-type specific manner  
566 (Bruno et al., 2019; Cosby et al., 2019; Ecco et al., 2017; Imbeault et al., 2017). For  
567 example, there is evidence that the progenitors of the currently active L1HS subfamily  
568 became silenced in human ESCs via KZFP targeting, but evaded that repression and  
569 persisted in that niche through the deletion of the KZFP binding site (Jacobs et al.,  
570 2014). HERVH may have persisted through another evasive strategy: changing their  
571 TFBS repertoire to colonize niches lacking their repressors. To silence all LTR7, any  
572 potential HERVH-targeting KZFP would need to gain expression in multiple cellular  
573 contexts. For example, one potential repressor, ZNF534, binds a wide range of LTR7  
574 sequences, but is particularly enriched at 7up in HEK293 cells (Fig. 3A,D). Our analysis  
575 shows that ZNF534 is most highly expressed in the morula, but dips in human ESC  
576 (Figure supplement 3). Thus, ZNF534 may repress 7up at earlier stages of development

577 but is apparently unable to suppress 7up transcription in pluripotent stem cells. If true,  
578 this scenario would illustrate how LTR diversification facilitated HERVH persistence in  
579 the face of KZFP coevolution. Further investigation is needed to explore the interplay  
580 between KZFPs and HERVH subfamilies during primate evolution.

581

## 582 **Implications for stem cell and regenerative biology**

583 Lastly, our findings may provide new opportunities for stem cell research and  
584 regenerative medicine. Our data on 7up reinforces previous findings (Corsinotti et al.,  
585 2017; Wang et al., 2012) that place SOX2/3 as central players in pluripotency.  
586 Furthermore, our analysis identified a set of TFs whose motifs are uniquely enriched in  
587 different LTR7 subfamilies with distinct expression patterns in early embryonic cells,  
588 which may enable a functional discriminatory analysis of the role of these TFs in each  
589 cell type. HERVH/LTR7 has been used as a marker for human pluripotency (Ohnuki et  
590 al., 2014; Santoni et al., 2012; Wang et al., 2014), and recent work has revealed that  
591 HERVH/LTR7-positive cells may be more amenable to differentiation, and are therefore  
592 referred to as “primed” cells (Göke et al., 2015; Theunissen et al., 2016). However,  
593 primed cells are not as promising for regenerative medicine as so-called “naïve” cells  
594 (Nichols and Smith, 2009), which are less differentiated and resemble cells from late  
595 morula to epiblast, or so-called “formative” cells, which most closely resemble cells from  
596 the early post-implantation epiblast (Kalkan and Smith, 2014; Kinoshita et al., 2021;  
597 Rossant and Tam, 2017). Of relevance to this issue is our finding that elements of the  
598 7u2 subfamily are highly and exclusively expressed in the pluripotent epiblast in vivo  
599 (Fig. 5), but weakly so in H1 ESC, which consists of a majority of primed cells and a  
600 minority of naïve or formative cells (Gafni et al., 2013). Thus, it might be possible to  
601 develop a LTR7u2-driven reporter system to mark and purify naïve or formative cells  
602 from an heterogenous ESC population. Similarly, a MERVL LTR-GFP transgene has  
603 been used in mouse to purify rare 2-cell-like totipotent cells where this LTR is  
604 specifically expressed amidst mouse ESCs in culture (Hermant and Torres-Padilla,  
605 2021; Macfarlan et al., 2012).

606 In conclusion, our study highlights the modular cis-regulatory evolution of an  
607 endogenous retrovirus which has facilitated its transcriptional partitioning in early  
608 embryogenesis. We believe that phyloregulatory dissection of endogenous retroviral  
609 LTRs has the potential to further our understanding of the evolution, impact, and  
610 applications of these elements in a broad range of biomedical areas.

611 **Acknowledgements:**

612 We would like to thank Arian Smit and Robert Hubley for their assistance in remasking  
613 the human genome with the custom LTR7 library in accordance with  
614 RepeatMasker/Dfam specifications. We would also like to thank the Cornell statistical  
615 consulting unit (CSCU), and Stephen Parry in particular, for their help with statistical  
616 analyses. Finally, we would like to credit BioRender.com for its primate (Fig. 2,7) and  
617 embryonic cell (Fig. 6,7) graphics. This work was supported by funds from the National  
618 Institutes of Health to CF (GM112972; HG009391; GM122550); Cornell Center for  
619 Vertebrate Genomics to T.A.C.; and the Cornell Presidential Fellow Program to M.S.  
620 J.L.R. is supported by the Howard Hughes Medical Institute Faculty Scholar program  
621 and NIH (GM099117).

## 622 **Methods**

### 623 HERVH LTR sequence identification:

624 All HERVH-int and accompanying LTRs (LTR7, 7b, 7c, and 7y) were extracted from  
625 masked (RepeatMasker version 4.0.5 repeat Library 20140131 - (Smit et al., 2013))  
626 GRCh38/hg38 (alt chromosomes removed). All annotated HERVH-int and HERVH LTR  
627 were run through OneCodeToFindThemAll.pl (Bailly-Bechet et al., 2014) followed by  
628 rename\_mergedLTRelements.pl (Thomas et al., 2018) to identify solo and full-length  
629 HERVH insertions. 5' LTRs from full-length insertions >4kb were combined with and  
630 solo LTRs. LTRs >350bp were considered for future analysis.

### 631 Multiple sequence alignment, phylogenetic tree generation, and LTR7 subdivision:

632 All HERVH LTRs (Fig. 1A – supp. file 5) or only LTR7s (Fig. 1B – supp. file 6) were  
633 aligned with mafft –auto (Nakamura et al., 2018) strategy: FFT-NS-2/Progressive  
634 method followed by PRANK (Löytynoja and Goldman, 2010) with options -showanc -  
635 support -njtree -uselogs -prunetree -prunedata -F -showevents. Uninformative structural  
636 variations were removed with Trimal (Capella-Gutierrez et al., 2009) with option -gt  
637 0.01.

638 To visualize inter-insertion relationships, the MSA was input into IQtree with options -nt  
639 AUTO -m MFP -bb 6000 -asr -minsup .95 (Chernomor et al., 2016). This only displays  
640 nodes with ultrafast (UF) bootstrap support >0.95.

641 Clusters of >10 insertions sharing a node with UFbootstrap support that were separated  
642 from other insertions by internal branch lengths >0.015 (1.5subs / 100 bp) were defined  
643 as belonging to a new bona fide LTR7 subfamily (Fig. 1B).

### 644 LTR7 consensus generation and network analysis:

645 Majority rule (51%) was used to generate each LTR7 subfamily at nodes described in  
646 Fig. 1. Positions without majority consensus are listed as “N”. Majority rule consensus  
647 sequences were aligned with MUSCLE in SEAVIEW (supp. file 7) (Edgar, 2004; Gouy  
648 et al., 2010). Alignment was visualized with Jalview2 (Waterhouse et al., 2009)(Fig. 4A)  
649 and ggplot2 (Fig. 4).

650 Non-gap SNPs from the muscle alignment were used to construct a median-joining  
651 network (Bandelt et al., 1999) with POPART (Leigh and Bryant, 2015).

652 Reverse Transcriptase Domain extraction, alignment, and tree generation:

653 The reverse transcriptase (RT) domain was extracted from HERVH-int consensus via  
654 reprobrowser (Fernandes et al., 2020):

```
655 CACCCTTACCCCGCTCAATGCCAATATCCCATCCCACAGCATGCTTTAAAAGGATT  
656 AAAGCCTGTTATCACTCGCCTGCTACAGCATGGCCTTTTAAAGCCTATAAACTCTCC  
657 TTACAATTCCCCCATTTTACCTGTCCTAAAACCAGACAAGCCTTACAAGTTAGTTCA  
658 GGATCTGTGCCTTATCAACCAATTGTTTTGCCTATCCACCCCATGGTGCCAAACC  
659 CATATACTCTCCTATCCTCAATACCTCCCTCCACAACCCATTATTCTGTTCTGGATC  
660 TCAAACATGCTTTCTTTACTATTCTTTGCACCCTTCATCCCAGCCTCTCTTCGCTTT  
661 CACTTGGA
```

662 This sequence was blasted (best hit) against all annotated HERVH-int in the human  
663 genome and matches were extracted. Corresponding LTR7 subdivision annotations  
664 from figure 1 were matched with these HERVH-int RT domains. Mafft alignment and  
665 IQTree generation were done identically to the Mafft and IQTree run for the LTRs (see  
666 corresponding methods section).

667 Peak calling:

668 ChIP-seq datasets representing transcription factors (TFs), histone modifications, and  
669 regulatory complexes in human embryonic stem cells and differentiated cells were  
670 retrieved from GSE61475 (38 distinct TFs and histone modifications), GSE69647  
671 (H3K27Ac, POU5F1, MED1 and CTCF), GSE117395 (H3K27Ac, H3K9Me3, KLF4, and  
672 KLF17), and GSE78099 (An array of KRAB-ZNFs and TRIM28) (Imbeault et al., 2017).  
673 ZNFs enriched in LTR7 binding (ZNF90, ZNF534, ZNF75, ZNF69B, ZNF257, ZNF57,  
674 and ZNF101) from HEK293 peaks were all evaluated, but only ZNF90 and ZNF534  
675 bound >100 LTR7 insertions (data not shown). The others were dropped from the  
676 analysis.



677 ChIP-seq reads were aligned to the hg19 human reference genome using the Bowtie2.  
678 All reads with phred score less than 33 and PCR duplicates were removed using  
679 bowtie2 and Picard tools respectively. ChIP-seq peaks were called by MACS2 with the  
680 parameters in “narrow” mode for TFs and “broad” mode for histone modifications,  
681 keeping FDR < 1%. ENCODE-defined blacklisted regions were excluded from called  
682 peaks. For phyloregulatory analysis (Fig. 2), we then converted hg19 to hg38 (no alt)  
683 coordinates via UCSC *liftover* (100% of coordinates lifted) and intersected these peak  
684 with the loci from LTR7 subfamilies using bedtools with any overlap. For ChIP-seq  
685 binding enrichment on a subset of marks following motif analysis (Fig 5), 70% overlap of  
686 peak and LTR was required. Enrichment of a given TF within LTR7 subfamilies was  
687 calculated using enrichR package in R, using the customized in-house codes (see the  
688 codes on GitHub for the detailed analysis pipelines and calculation of enrichment  
689 score).

#### 690 Phyloregulatory analysis:

691 Peaks from external ChIP-seq datasets were intersected with LTR7 insertions (Quinlan  
692 and Hall, 2010). LTR7 insertions that intersected with >1bp of peaks were counted as  
693 positive for the respective mark. We repeated this analysis with a range of overlap  
694 requirements from extending the LTR 500bp into unique DNA to 70% overlap and found  
695 few differential calls (data not shown). The phylogenetic tree rooted on 7b (ggtree) was  
696 combined with these binary data (ggheat).

697 “Highly transcribed” (fpkm >2) and “chimeric” HERVH from H1 cells (GSE54726) (Wang  
698 et al., 2014) were intersected with LTR7 similarly to ChIP-seq data. Those which  
699 intersected LTR7 were marked as “RNA-seq” or “chimeric” respectively. GRO-seq  
700 profiles from H1 cells (Estaras et al.) (GSE64758) were created for windows 10bp  
701 upstream and 8kb downstream of 5’ and solo LTR7 (Ramírez et al., 2016). The most  
702 visible signal was confined to the top 7<sup>th</sup> of insertions (Figure supplement 2). All LTR7  
703 were subdivided into septiles, due to visible signal being confined to the top 7<sup>th</sup> of  
704 insertions; those of the top septile were labeled “GRO-seq”.

#### 705 Peak proportion heatmap generation and statistical analysis:

706 Tables with the proportion of solo and 5' LTRs from a given subfamily positive for select  
707 marks (phyloregulatory analysis) were used to generate heatmaps with the R package  
708 ggplot (ggheat) (Ginestet, 2011). Those with  $p_{adj} < 0.05$  (Chi-square Bonferroni  
709 correction  $n=147$  tests for a total of 21 marks examined) were considered significantly  
710 enriched in 7up1. Enrichment for non-LTR7up subfamilies was not tested. While not all  
711 tested marks are displayed in the main text, statistical analysis was performed with all  
712 tested marks ( $n=147$ ) (supp. file 8). For comparing transcribed 7up to untranscribed  
713 7up, 18 pairwise comparisons were made (supp. file 9).

#### 714 Aggregate signal heatmap generation:

715 GRO-seq (H1 cells - GSE64758), whole-genome bisulfite sequencing (WGBS-seq – H1  
716 cells), and H3K9me3 ChIP-seq (H1 – primed - GSE78099) bams were retrieved from  
717 (Estarás et al., 2015), (Dunham et al., 2012), and (Theunissen et al., 2016) respectively.  
718 Deeptools (Ramírez et al., 2016) was used to visualize these marks by LTR7 subfamily  
719 division in windows 10bp upstream and 8kb downstream of the most 5' position in the  
720 LTR (Figure supplement 2).

#### 721 Orthologous insertion aging:

722 Human coordinates for 7b, 7c, and 7y and LTR7 used in alignments and tree generation  
723 were lifted over (Kent et al., 2002; Raney et al., 2014) from GRCh38/hg38 (Miga et al.,  
724 2014) to Clint\_PTRv2/panTro6 (Waterson et al., 2005), Kamilah\_GGO\_v0/gorGor6  
725 (Scally et al., 2012), Susie\_PABv2/ponAbe3 (Locke et al., 2011), GGSC  
726 Nleu3.0/nomLeu3 (Carbone et al., 2014), or Mmul\_10/rheMac10 (Gibbs et al., 2007).  
727 Those that were successfully lifted over from human to non-human primate were then  
728 lifted over back to human. Only those that survived both liftovers (1:1 orthologous) were  
729 counted as present in non-human primates. The proportion of those orthologous to  
730 human and total number of orthologous was plotted with ggplot2.

#### 731 Terminal branch length aging:

732 Terminal branch lengths from the LTR7 phylogenetic tree (Fig. 1B) were extracted and  
733 plotted with ggplot2. Similarly aged subfamilies were inferred from means here and from  
734 orthologous insertion aging for statistical testing. Three total groups were tested for

735 differences in means (7up1/7up2/7u2 vs. 7d1/7d2/7u1 vs. 7bc/o) via Wilcox rank-sum  
736 test with Bonferroni multiple testing correction.

737 Identification of recombination breakpoints and consensus parsimony tree generation:

738 Major recombination breakpoints were identified by eye from the consensus sequence  
739 MSA, where SNPs and structural rearrangements seemed to have different  
740 relationships between blocks. Putative block recombination events were identified by  
741 looking for shared shapes in the block consensus MSA (Fig. 4A). To test if these were  
742 truly recombination events and could not be explained by evolution by common  
743 descent, inter-block sequence relationship differences were tested by generating  
744 parsimony trees and comparing these to the overall phylogenetic structure from Fig. 1A.  
745 Parsimony trees were generated in SEAVIEW, treating all gaps as unknown states  
746 (except in the case of 2b, where the entire sequence is gaps and gaps were not treated  
747 differently than other sequence), bootstrapped 5000 times with the option “more  
748 thorough tree search”. Differences in block parsimony trees and the overall phylogeny  
749 that had bootstrap support were marked in red and included in Fig. 4D,7.

750 7up consensus block 2a 2b alignment and parsimony tree:

751 LTR7up blocks 2a and 2b (Fig. 4) appeared to share sequence. To determine if block  
752 2b was the result of a duplication of 2a, we extracted these sequences from the  
753 LTR7up1 consensus and aligned them with blastn (NCBI web version) with default  
754 settings. To determine the relationship of all HERVH LTR 2a and 2b blocks, we  
755 performed a muscle alignment (default settings) of all 2a and 2b from all HERVH LTR  
756 consensus sequences and then generated a parsimony tree with 5000 bootstraps with  
757 SEAVIEW with the option “more thorough tree search”.

758 New LTR7B/C/Y consensus generation and remasking of human genome:

759 Consensus sequences for LTR7 subfamilies were generated using the tree from figure  
760 1b (see above). For LTR7b/c/y, we used the alignment and tree comprising all HERVH  
761 LTR (Figure supplement 5). To do this, we identified nodes with >0.95 ultrafast  
762 bootstrap support that were comprised of predominately (>90%) of previously annotated  
763 LTR7b, LTR7c, or LTR7y. These sequences were used to generate majority-rule

764 consensus sequences for their respective subfamily. We generated 2 mutually-  
765 exclusive LTR7c consensus sequences (LTR7C1 and LTR7C2) due to the high  
766 sequence divergence of LTR7C. Both of these subfamilies were merged into “LTR7C”  
767 after remasking.

768 Parsing previously annotated LTR7 into 8 subfamilies and evidence of recurrent  
769 recombination events caused concern that HERVH LTRs may be misannotated in the  
770 repeat masker annotations. To compensate, we remasked (Smit et al., 2013)  
771 GRCh38/hg38 (excluding alt chromosomes) with a custom library consisting of the new  
772 consensus sequences for LTR7 subfamilies, new consensus sequences for 7b, 7y, and  
773 7c (see above) based on the HERVH LTR tree from Fig. 4, and HERVH-int (dfam). We  
774 also included annotated consensus sequences from dfam for MER48, MER39, AluYk3,  
775 and MST1N2, who we found a HERVH only library also masked to a limited degree  
776 (data not shown). With this library, we ran RepeatMasker with crossmatch and  
777 “sensitive” settings: -e crossmatch -a -s -no\_is. Changes in annotations can be found in  
778 (HERVH\_LTRremasking.xlsx)

#### 779 Embryonic HERVH subfamily expression analysis:

780 We downloaded the raw single-cell RNA-seq datasets from early human embryos and  
781 embryonic stem cells (GSE36552) and the EPI, PE, TE cells (GSE66507) in sra format.  
782 Following the conversion of raw files into fastq format, the quality was determined by  
783 using the FastQC. We removed two nucleotides from the ends as their quality scores  
784 were highly variable compared with the rest of the sequences in RNA-seq reads. Prior  
785 to aligning the resulting reads, we first curated the reference genome annotations using  
786 the LTR7 classification, shown in the manuscript. We extracted the genes (genecode  
787 V19), and LTR7 subfamilies (see figure 5) genomic sequences and combined them to  
788 generate a reference transcriptome. These sequences were then appended, comprising  
789 the coding-sequences plus UTRs of genes and locus-level LTR7 subfamilies sequences  
790 in fasta format. We then annotated every fasta sequences with their respective genes or  
791 LTR7 subfamilies IDs. To guide the transcriptome assembly, we also appended the  
792 each of the resulting contigs and modelled them in gtf format that we utilized for the  
793 expression quantification. Next, we indexed the concatenated genes and LTR7

794 subfamilies transcriptome and genome reference sequences using ‘salmon’ (Patro et  
795 al., 2017). Finally, we aligned the trimmed sequencing reads against the curated  
796 reference genome. The ‘salmon’ tool quantified the counts and normalized expression  
797 (Transcripts per million (TPM)) for each single cell RNAseq sample. Overall, this  
798 approach enabled us to simultaneously calculate LTR7 subfamilies and protein-coding  
799 gene expression using expected maximization algorithms. Data integration of obtained  
800 count matrix, normalization at logarithmic scale, and scaling were performed as per the  
801 “Seurat V.3.7” (<http://satijalab.org/seurat/>) guidelines. The annotations of cell-types were  
802 taken as it was classified in original studies. We calculated differential expression and  
803 tested their significance level using Kruskal–Wallis test by comparing cell-types of  
804 interest with the rest of the cells. The obtained p-values were further adjusted by the  
805 Benjamini-Hochberg method to calculate the False Discovery Rate (FDR). All the  
806 statistics and visualization of RNA-seq were performed on R (<https://www.r-project.org/>).

#### 807 Motif Enrichment:

808 For each subfamily of LTR7 elements, all re-annotated elements were aligned against  
809 the subfamily consensus sequence using MUSCLE (Edgar, 2004). These multiple-  
810 sequence alignments were then split based on the recombination block positions in the  
811 consensus sequence. The consensus sequence was then removed. Binding motif  
812 position-weight matrices were downloaded from HOMER (Heinz et al., 2010) and were  
813 used to perform pairwise motif enrichment using the command ‘homer2 find’. For  
814 LTR7up1 enrichment (Fig. 6A - testing which motifs were enriched in LTR7up1  
815 compared to other subfamilies), enrichment was only calculated for LTR7up1 and the  
816 motifs with a  $-\log(p\text{-value})$  cutoff of  $1 \times 10^{-5}$  were kept. For enrichment in all subfamilies  
817 (supp. files 3,4) – testing all subfamilies against all others), every pairwise subfamily  
818 combination within each block was tested and all results are displayed.

819

#### 820 SOX2 ChIP-seq signal on LTR7:

821 SOX2 ChIP-seq and whole-cell extract datasets from primed hESCs were downloaded  
822 in fastq format from GEO ID GSE125553 (Bayerl et al., 2021). Fastq reads were  
823 mapped against the hg19 reference genome with the bowtie2 parameters: *–very-*

824 *sensitive-local*. All unmapped reads with Phred score < 33 and putative PCR duplicates  
825 were removed using *Picard* and *samtools*. All the ChIP-seq narrow peaks were called  
826 by MACS2 (FDR < 0.01). To generate a set of unique peaks, we merged ChIP-seq  
827 peaks within 50 bp of one another using the *mergeBed* function from *bedtools*. We then  
828 intersected these peak sets with LTR7 subgroups from hg19 repeat-masked  
829 coordinates using *bedtools intersectBed* with 50% overlap. LTR7up1 and LTR7up2  
830 were harboring the highest number of peaks compared with the rest of the subgroups.  
831 To illustrate the enrichment over the LTR7 subgroups, we first extended 500 basepairs  
832 from upstream and downstream coordinates from the left boundary of each  
833 LTR7subgroups. These 1KB windows were further divided into 10 bps bins. The  
834 normalized ChIP-seq signal over the local lambda (piled up *bedGraph* outputs from  
835 MACS2) was counted in each bin. These counts were then normalized by the total  
836 number of mappable reads per million in given samples and presented as signal per  
837 million per 10 bps. Finally, these values were averaged across the loci for each bin to  
838 illustrate the subfamilies' level of ChIP-seq enrichment. Replicates were merged prior to  
839 plotting. Note: Pearson's correlation coefficient between replicates across the bins was  
840 found to be  $r > 0.90$ .

841

#### 842 Luciferase reporter assay:

843 The inserts (LTR7 variants or EF1a promoter) with restriction enzyme overhangs were  
844 ordered from Genewiz and cloned into pGL3-basic plasmid upstream of the firefly  
845 reporter gene (E1751, Promega). Minipreps were prepared with QIAprep Spin Miniprep  
846 kit (Qiagen). Plasmids were sequenced to ensure the correct sequence and  
847 directionality of the insert. 24 h before transfection, human iPSC WTC-11 (Coriell  
848 Institute) cells were plated on Vitronectin (Thermo Fisher Scientific) coated 12-well  
849 plates in Essential 8 Flex medium (Thermo Fisher Scientific) with E8 supplement  
850 (Thermo Fisher Scientific), Rock inhibitor and 2.5% penicillin-streptomycin. Cells were  
851 co-transfected with 800 ng of plasmid of interest and 150 ng plasmid containing EF1a  
852 upstream of GFP for normalization with Lipofectamine Stem transfection reagent  
853 (Thermo Fisher scientific) according to manufacturer's instructions. 48 h after

854 transfection, cell pellet was harvested and luciferase activity was measured with  
855 Luciferase Reporter Assay kit (Promega) on Glomax (Promega) according to  
856 instructions. Transfection efficiency and cell count was normalized with GFP.

857 1. 7down:

858 **GCTAGC**TGTCAGGCCTCTGAGCCCAAGCTAAGCCATCATATCCCCTGTGACCTGC  
859 ACGTACACATCCAGATGGCCGGTTCCTGCCTTAACTGATGACATTCCACCACAAAA  
860 GAAGTGAAAATGGCCTGTTCCCTGCCTTAACTGATGACATTATCTTGTGAAATTCCTT  
861 CTCCTGGCTCATCCTGGCTCAAAGCTCCCCTACTGAGCACCTTGTGACCCCCACT  
862 CCTGCCCGCCAGAGAACAACCCCCCTTTGACTGTAATTTTCCTTTACCTACCCAAA  
863 TCCTATAAAACGGCCCCACCCCTATCTCCCTTCGCTGACTCTCTTTTCGGACTCAG  
864 CCCGCCTGCACCCAGGTGAAATAAACAGCTTTATTGCTCACACAAAGCCTGTTTGG  
865 TGGTCTCTTCACACGGACGCGCATG**CTCGAG**

866 2. LTR7upcons:

867 **GCTAGC**TGTCAGGCCTCTGAGCCCAAGCCAAGCCATCGCATCCCCTGTGACTTGC  
868 ACGTATACGCCCAGATGGCCTGAAGTAACTGAAGAATCACAAAAGAAGTGAATATG  
869 CCCTGCCCCACCTTAACTGATGACATTCCACCACAAAAGAAGTGTAATGGCCGGT  
870 CCTTGCCTTAAGTGAATGACATTACCTTGTGAAAGTCCTTTTCCTGGCTCATCCTGGC  
871 TCAAAAAGCACCCCCACTGAGCACCTTGCACCCCCACTCCTGCCCGCCAGAGAA  
872 CAAACCCCCTTTGACTGTAATTTTCCTTTACCTACCCAAATCCTATAAAACGGCCCC  
873 ACCCTTATCTCCCTTCGCTGACTCTCTTTTCGGACTCAGCCCGCCTGCACCCAGGT  
874 GAAATAAACAGCCATGTTGCTCACACAAAGCCTGTTTGGTGGTCTCTTCACACGGA  
875 CGCGCATG**CTCGAG**

876 5. LTR7upcons\_AAAGAAG\_deletion:

877 **GCTAGC**TGTCAGGCCTCTGAGCCCAAGCCAAGCCATCGCATCCCCTGTGACTTGC  
878 ACGTATACGCCCAGATGGCCTGAAGTAACTGAAGAATCACAAAAGAAGTGAATATG  
879 CCCTGCCCCACCTTAACTGATGACATTCCACCATTGTAATGGCCGGTCTTGCCT  
880 TAAGTGAATGACATTACCTTGTGAAAGTCCTTTTCCTGGCTCATCCTGGCTCAAAAAG

881 CACCCCACTGAGCACCTTGCGACCCCACTCCTGCCCGCCAGAGAACAACCCC  
882 CTTTGACTGTAATTTTCCTTTACCTACCCAAATCCTATAAAACGGCCCCACCCTTAT  
883 CTCCCTTCGCTGACTCTCTTTTCGGACTCAGCCCGCCTGCACCCAGGTGAAATAAA  
884 CAGCCATGTTGCTCACACAAAGCCTGTTTGGTGGTCTCTTCACACGGACGCGCAT  
885 GCTCGAG

886 5'NheI highlighted in Yellow

887 3'XhoI highlighted in Cyan



- 888 Babaian A, Mager DL. 2016. Endogenous retroviral promoter exaptation in human cancer. *Mobile DNA*  
889 **7**:24. doi:10.1186/s13100-016-0080-x
- 890 Bailly-Bechet M, Haudry A, Lerat E. 2014. “One code to find them all”: a perl tool to conveniently parse  
891 RepeatMasker output files. *Mobile DNA* **5**:13. doi:10.1186/1759-8753-5-13
- 892 Bandelt HJ, Forster P, Röhl A. 1999. Median-joining networks for inferring intraspecific phylogenies.  
893 *Molecular Biology and Evolution* **16**:37–48. doi:10.1093/oxfordjournals.molbev.a026036
- 894 Bannert N, Kurth R. 2004. Retroelements and the human genome: New perspectives on an old relation.  
895 *PNAS* **101**:14572–14579. doi:10.1073/pnas.0404838101
- 896 Bao W, Kojima KK, Kohany O. 2015. Repbase Update, a database of repetitive elements in eukaryotic  
897 genomes. *Mobile DNA* **6**:11. doi:10.1186/s13100-015-0041-9
- 898 Bayerl J, Ayyash M, Shani T, Manor YS, Gafni O, Massarwa R, Kalma Y, Aguilera-Castrejon A, Zerbib M,  
899 Amir H, Sheban D, Geula S, Mor N, Weinberger L, Naveh Tassa S, Krupalnik V, Oldak B, Livnat N, Tarazi S,  
900 Tawil S, Wildschutz E, Ashoukhi S, Lasman L, Rotter V, Hanna S, Ben-Yosef D, Novershtern N, Viukov S,  
901 Hanna JH. 2021. Principles of signaling pathway modulation for enhancing human naive pluripotency  
902 induction. *Cell Stem Cell* S1934-5909(21)00158–2. doi:10.1016/j.stem.2021.04.001
- 903 Bergsland M, Ramsköld D, Zaouter C, Klum S, Sandberg R, Muhr J. 2011. Sequentially acting Sox  
904 transcription factors in neural lineage development. *Genes Dev* **25**:2453–2464.  
905 doi:10.1101/gad.176008.111
- 906 Blakeley P, Fogarty NME, del Valle I, Wamaita SE, Hu TX, Elder K, Snell P, Christie L, Robson P, Niakan  
907 KK. 2015. Defining the three cell lineages of the human blastocyst by single-cell RNA-seq. *Development*  
908 **142**:3151–3165. doi:10.1242/dev.123547
- 909 Boyer LA, Lee TI, Cole MF, Johnstone SE, Levine SS, Zucker JP, Guenther MG, Kumar RM, Murray HL,  
910 Jenner RG, Gifford DK, Melton DA, Jaenisch R, Young RA. 2005. Core Transcriptional Regulatory Circuitry  
911 in Human Embryonic Stem Cells. *Cell* **122**:947–956. doi:10.1016/j.cell.2005.08.020
- 912 Bruno M, Mahgoub M, Macfarlan TS. 2019. The Arms Race Between KRAB–Zinc Finger Proteins and  
913 Endogenous Retroelements and Its Impact on Mammals. *Annual Review of Genetics* **53**:393–416.  
914 doi:10.1146/annurev-genet-112618-043717
- 915 Capella-Gutierrez S, Silla-Martinez JM, Gabaldon T. 2009. trimAl: a tool for automated alignment  
916 trimming in large-scale phylogenetic analyses. *Bioinformatics* **25**:1972–1973.  
917 doi:10.1093/bioinformatics/btp348
- 918 Carbone L, Alan Harris R, Gnerre S, Veeramah KR, Lorente-Galdos B, Huddleston J, Meyer TJ, Herrero J,  
919 Roos C, Aken B, Anaclerio F, Archidiacono N, Baker C, Barrell D, Batzer MA, Beal K, Blancher A, Bohrsen  
920 CL, Brameier M, Campbell MS, Capozzi O, Casola C, Chiatante G, Cree A, Damert A, de Jong PJ, Dumas L,  
921 Fernandez-Callejo M, Flicek P, Fuchs NV, Gut I, Gut M, Hahn MW, Hernandez-Rodriguez J, Hillier LW,  
922 Hubley R, Ianc B, Izsvák Z, Jablonski NG, Johnstone LM, Karimpour-Fard A, Konkel MK, Kostka D, Lazar  
923 NH, Lee SL, Lewis LR, Liu Y, Locke DP, Mallick S, Mendez FL, Muffato M, Nazareth LV, Nevenon KA,  
924 O’Bleness M, Ochis C, Odom DT, Pollard KS, Quilez J, Reich D, Rocchi M, Schumann GG, Searle S, Sikela  
925 JM, Skollar G, Smit A, Sonmez K, Hallers B ten, Terhune E, Thomas GWC, Ullmer B, Ventura M, Walker JA,

- 926 Wall JD, Walter L, Ward MC, Wheelan SJ, Whelan CW, White S, Wilhelm LJ, Woerner AE, Yandell M, Zhu  
927 B, Hammer MF, Marques-Bonet T, Eichler EE, Fulton L, Fronick C, Muzny DM, Warren WC, Worley KC,  
928 Rogers J, Wilson RK, Gibbs RA. 2014. Gibbon genome and the fast karyotype evolution of small apes.  
929 *Nature* **513**:195–201. doi:10.1038/nature13679
- 930 Chambers I, Smith A. 2004. Self-renewal of teratocarcinoma and embryonic stem cells. *Oncogene*  
931 **23**:7150–7160. doi:10.1038/sj.onc.1207930
- 932 Chang N-C, Rovira Q, Wells JN, Feschotte C, Vaquerizas JM. 2021. A genomic portrait of zebrafish  
933 transposable elements and their spatiotemporal embryonic expression. *bioRxiv* 2021.04.08.439009.  
934 doi:10.1101/2021.04.08.439009
- 935 Charlesworth B, Langley CH. 1986. THE EVOLUTION OF SELF-REGULATED TRANSPOSITION OF  
936 TRANSPOSABLE ELEMENTS. *Genetics* **112**:359–383.
- 937 Chernomor O, von Haeseler A, Minh BQ. 2016. Terrace Aware Data Structure for Phylogenomic  
938 Inference from Supermatrices. *Systematic Biology* **65**:997–1008. doi:10.1093/sysbio/syw037
- 939 Chuong EB, Elde NC, Feschotte C. 2017. Regulatory activities of transposable elements: from conflicts to  
940 benefits. *Nat Rev Genet* **18**:71–86. doi:10.1038/nrg.2016.139
- 941 Chuong EB, Elde NC, Feschotte C. 2016. Regulatory evolution of innate immunity through co-option of  
942 endogenous retroviruses. *Science* **351**:1083–1087. doi:10.1126/science.aad5497
- 943 Cordaux R, Hedges DJ, Batzer MA. 2004. Retrotransposition of Alu elements: how many sources? *Trends*  
944 *in Genetics* **20**:464–467. doi:10.1016/j.tig.2004.07.012
- 945 Corsinotti A, Wong FC, Tatar T, Szczerbinska I, Halbritter F, Colby D, Gogolok S, Pantier R, Liggat K,  
946 Mirfazeli ES, Hall-Ponsole E, Mullin NP, Wilson V, Chambers I. 2017. Distinct SoxB1 networks are  
947 required for naïve and primed pluripotency. *eLife* **6**:e27746. doi:10.7554/eLife.27746
- 948 Cosby RL, Chang N-C, Feschotte C. 2019. Host–transposon interactions: conflict, cooperation, and  
949 cooption. *Genes Dev* **33**:1098–1116. doi:10.1101/gad.327312.119
- 950 Deniz Ö, Ahmed M, Todd CD, Rio-Machin A, Dawson MA, Branco MR. 2020. Endogenous retroviruses are  
951 a source of enhancers with oncogenic potential in acute myeloid leukaemia. *Nat Commun* **11**:3506.  
952 doi:10.1038/s41467-020-17206-4
- 953 Dunham I, Kundaje A, Aldred SF, Collins PJ, Davis CA, Doyle F, Epstein CB, Frietze S, Harrow J, Kaul R,  
954 Khatun J, Lajoie BR, Landt SG, Lee B-K, Pauli F, Rosenbloom KR, Sabo P, Safi A, Sanyal A, Shores N,  
955 Simon JM, Song L, Trinklein ND, Altshuler RC, Birney E, Brown JB, Cheng C, Djebali S, Dong X, Dunham I,  
956 Ernst J, Furey TS, Gerstein M, Giardine B, Greven M, Hardison RC, Harris RS, Herrero J, Hoffman MM,  
957 Iyer S, Kellis M, Khatun J, Kheradpour P, Kundaje A, Lassmann T, Li Q, Lin X, Marinov GK, Merkel A,  
958 Mortazavi A, Parker SCJ, Reddy TE, Rozowsky J, Schlesinger F, Thurman RE, Wang J, Ward LD, Whitfield  
959 TW, Wilder SP, Wu W, Xi HS, Yip KY, Zhuang J, Bernstein BE, Birney E, Dunham I, Green ED, Gunter C,  
960 Snyder M, Pazin MJ, Lowdon RF, Dillon LAL, Adams LB, Kelly CJ, Zhang J, Wexler JR, Green ED, Good PJ,  
961 Feingold EA, Bernstein BE, Birney E, Crawford GE, Dekker J, Elnitski L, Farnham PJ, Gerstein M, Giddings  
962 MC, Gingeras TR, Green ED, Guigó R, Hardison RC, Hubbard TJ, Kellis M, Kent WJ, Lieb JD, Margulies EH,  
963 Myers RM, Snyder M, Stamatoyannopoulos JA, Tenenbaum SA, Weng Z, White KP, Wold B, Khatun J, Yu

- 964 Y, Wrobel J, Risk BA, Gunawardena HP, Kuiper HC, Maier CW, Xie L, Chen X, Giddings MC, Bernstein BE,  
965 Epstein CB, Shores N, Ernst J, Kheradpour P, Mikkelsen TS, Gillespie S, Goren A, Ram O, Zhang X, Wang  
966 L, Issner R, Coyne MJ, Durham T, Ku M, Truong T, Ward LD, Altshuler RC, Eaton ML, Kellis M, Djebali S,  
967 Davis CA, Merkel A, Dobin A, Lassmann T, Mortazavi A, Tanzer A, Lagarde J, Lin W, Schlesinger F, Xue C,  
968 Marinov GK, Khatun J, Williams BA, Zaleski C, Rozowsky J, Röder M, Kokocinski F, Abdelhamid RF, Alioto  
969 T, Antoshechkin I, Baer MT, Batut P, Bell I, Bell K, Chakraborty S, Chen X, Chrast J, Curado J, Derrien T,  
970 Drenkow J, Dumais E, Dumais J, Dutttagupta R, Fastuca M, Fejes-Toth K, Ferreira P, Foissac S, Fullwood  
971 MJ, Gao H, Gonzalez D, Gordon A, Gunawardena HP, Howald C, Jha S, Johnson R, Kapranov P, King B,  
972 Kingswood C, Li G, Luo OJ, Park E, Preall JB, Presaud K, Ribeca P, Risk BA, Robyr D, Ruan X, Sammeth M,  
973 Sandhu KS, Schaeffer L, See L-H, Shahab A, Skancke J, Suzuki AM, Takahashi H, Tilgner H, Trout D,  
974 Walters N, Wang H, Wrobel J, Yu Y, Hayashizaki Y, Harrow J, Gerstein M, Hubbard TJ, Reymond A,  
975 Antonarakis SE, Hannon GJ, Giddings MC, Ruan Y, Wold B, Carninci P, Guigó R, Gingeras TR, Rosenbloom  
976 KR, Sloan CA, Learned K, Malladi VS, Wong MC, Barber GP, Cline MS, Dreszer TR, Heitner SG, Karolchik D,  
977 Kent WJ, Kirkup VM, Meyer LR, Long JC, Maddren M, Raney BJ, Furey TS, Song L, Grasfeder LL, Giresi PG,  
978 Lee B-K, Battenhouse A, Sheffield NC, Simon JM, Showers KA, Safi A, London D, Bhinge AA, Shestak C,  
979 Schaner MR, Ki Kim S, Zhang ZZ, Mieczkowski PA, Mieczkowska JO, Liu Z, McDaniell RM, Ni Y, Rashid NU,  
980 Kim MJ, Adar S, Zhang Z, Wang T, Winter D, Keefe D, Birney E, Iyer VR, Lieb JD, Crawford GE, Li G,  
981 Sandhu KS, Zheng M, Wang P, Luo OJ, Shahab A, Fullwood MJ, Ruan X, Ruan Y, Myers RM, Pauli F,  
982 Williams BA, Gertz J, Marinov GK, Reddy TE, Vielmetter J, Partridge E, Trout D, Varley KE, Gasper C, The  
983 ENCODE Project Consortium, Overall coordination (data analysis coordination), Data production leads  
984 (data production), Lead analysts (data analysis), Writing group, NHGRI project management (scientific  
985 management), Principal investigators (steering committee), Boise State University and University of  
986 North Carolina at Chapel Hill Proteomics groups (data production and analysis), Broad Institute Group  
987 (data production and analysis), Cold Spring Harbor U of G Center for Genomic Regulation, Barcelona,  
988 RIKEN, Sanger Institute, University of Lausanne, Genome Institute of Singapore group (data production  
989 and analysis), Data coordination center at UC Santa Cruz (production data coordination), Duke  
990 University E University of Texas, Austin, University of North Carolina-Chapel Hill group (data production  
991 and analysis), Genome Institute of Singapore group (data production and analysis), HudsonAlpha  
992 Institute C UC Irvine, Stanford group (data production and analysis). 2012. An integrated encyclopedia of  
993 DNA elements in the human genome. *Nature* **489**:57–74. doi:10.1038/nature11247
- 994 Ecco G, Imbeault M, Trono D. 2017. KRAB zinc finger proteins. *Development* **144**:2719–2729.  
995 doi:10.1242/dev.132605
- 996 Edgar RC. 2004. MUSCLE: multiple sequence alignment with high accuracy and high throughput. *Nucleic  
997 Acids Res* **32**:1792–1797. doi:10.1093/nar/gkh340
- 998 Eickbush TH, Malik HS. 2002. Origins and Evolution of Retrotransposons. *Mobile DNA II* 1111–1144.  
999 doi:10.1128/9781555817954.ch49
- 1000 Estarás C, Benner C, Jones KA. 2015. SMADs and YAP Compete to Control Elongation of  $\beta$ -Catenin:LEF-1-  
1001 Recruited RNAPII during hESC Differentiation. *Molecular Cell* **58**:780–793.  
1002 doi:10.1016/j.molcel.2015.04.001
- 1003 Faulkner GJ, Kimura Y, Daub CO, Wani S, Plessy C, Irvine KM, Schroder K, Cloonan N, Steptoe AL,  
1004 Lassmann T, Waki K, Hornig N, Arakawa T, Takahashi H, Kawai J, Forrest ARR, Suzuki H, Hayashizaki Y,

- 1005 Hume DA, Orlando V, Grimmond SM, Carninci P. 2009. The regulated retrotransposon transcriptome of  
1006 mammalian cells. *Nat Genet* **41**:563–571. doi:10.1038/ng.368
- 1007 Fernandes JD, Zamudio-Hurtado A, Clawson H, Kent WJ, Haussler D, Salama SR, Haeussler M. 2020. The  
1008 UCSC repeat browser allows discovery and visualization of evolutionary conflict across repeat families.  
1009 *Mobile DNA* **11**:13. doi:10.1186/s13100-020-00208-w
- 1010 Feschotte C. 2008. Transposable elements and the evolution of regulatory networks. *Nat Rev Genet*  
1011 **9**:397–405. doi:10.1038/nrg2337
- 1012 Fort A, Hashimoto K, Yamada D, Salimullah M, Keya CA, Saxena A, Bonetti A, Voineagu I, Bertin N, Kratz  
1013 A, Noro Y, Wong C-H, de Hoon M, Andersson R, Sandelin A, Suzuki H, Wei C-L, Koseki H, Hasegawa Y,  
1014 Forrest ARR, Carninci P. 2014. Deep transcriptome profiling of mammalian stem cells supports a  
1015 regulatory role for retrotransposons in pluripotency maintenance. *Nature Genetics* **46**:558–566.  
1016 doi:10.1038/ng.2965
- 1017 Gafni O, Weinberger L, Mansour AA, Manor YS, Chomsky E, Ben-Yosef D, Kalma Y, Viukov S, Maza I,  
1018 Zviran A, Rais Y, Shipony Z, Mukamel Z, Krupalnik V, Zerbib M, Geula S, Caspi I, Schneir D, Shwartz T,  
1019 Gilad S, Amann-Zalcenstein D, Benjamin S, Amit I, Tanay A, Massarwa R, Novershtern N, Hanna JH. 2013.  
1020 Derivation of novel human ground state naive pluripotent stem cells. *Nature* **504**:282–286.  
1021 doi:10.1038/nature12745
- 1022 Gemmell P, Hein J, Katzourakis A. 2019. The Exaptation of HERV-H: Evolutionary Analyses Reveal the  
1023 Genomic Features of Highly Transcribed Elements. *Front Immunol* **10**. doi:10.3389/fimmu.2019.01339
- 1024 Gemmell P, Hein J, Katzourakis A. 2015. Orthologous endogenous retroviruses exhibit directional  
1025 selection since the chimp-human split. *Retrovirology* **12**. doi:10.1186/s12977-015-0172-6
- 1026 Gibbs RA, Rogers J, Katze MG, Bumgarner R, Weinstock GM, Mardis ER, Remington KA, Strausberg RL,  
1027 Venter JC, Wilson RK, Batzer MA, Bustamante CD, Eichler EE, Hahn MW, Hardison RC, Makova KD, Miller  
1028 W, Milosavljevic A, Palermo RE, Siepel A, Sikela JM, Attaway T, Bell S, Bernard KE, Buhay CJ,  
1029 Chandrabose MN, Dao M, Davis C, Delehaunty KD, Ding Y, Dinh HH, Dugan-Rocha S, Fulton LA, Gabisi RA,  
1030 Garner TT, Godfrey J, Hawes AC, Hernandez J, Hines S, Holder M, Hume J, Jhangiani SN, Joshi V, Khan  
1031 ZM, Kirkness EF, Cree A, Fowler RG, Lee S, Lewis LR, Li Z, Liu Yih-shin, Moore SM, Muzny D, Nazareth LV,  
1032 Ngo DN, Okwuonu GO, Pai G, Parker D, Paul HA, Pfannkoch C, Pohl CS, Rogers Y-H, Ruiz SJ, Sabo A,  
1033 Santibanez J, Schneider BW, Smith SM, Sodergren E, Svatek AF, Utterback TR, Vattathil S, Warren W,  
1034 White CS, Chinwalla AT, Feng Y, Halpern AL, Hillier LW, Huang X, Minx P, Nelson JO, Pepin KH, Qin X,  
1035 Sutton GG, Venter E, Walenz BP, Wallis JW, Worley KC, Yang S-P, Jones SM, Marra MA, Rocchi M, Schein  
1036 JE, Baertsch R, Clarke L, Csürös M, Glasscock J, Harris RA, Havlak P, Jackson AR, Jiang H, Liu Yue, Messina  
1037 DN, Shen Y, Song HX-Z, Wylie T, Zhang L, Birney E, Han K, Konkel MK, Lee J, Smit AFA, Ullmer B, Wang H,  
1038 Xing J, Burhans R, Cheng Z, Karro JE, Ma J, Raney B, She X, Cox MJ, Demuth JP, Dumas LJ, Han S-G,  
1039 Hopkins J, Karimpour-Fard A, Kim YH, Pollack JR, Vinar T, Addo-Quaye C, Degenhardt J, Denby A, Hubisz  
1040 MJ, Indap A, Kosiol C, Lahn BT, Lawson HA, Marklein A, Nielsen R, Vallender EJ, Clark AG, Ferguson B,  
1041 Hernandez RD, Hirani K, Kehrer-Sawatzki H, Kolb J, Patil S, Pu L-L, Ren Y, Smith DG, Wheeler DA, Schenck  
1042 I, Ball EV, Chen R, Cooper DN, Giardine B, Hsu F, Kent WJ, Lesk A, Nelson DL, O'Brien WE, Prüfer K,  
1043 Stenson PD, Wallace JC, Ke H, Liu X-M, Wang P, Xiang AP, Yang F, Barber GP, Haussler D, Karolchik D,

- 1044 Kern AD, Kuhn RM, Smith KE, Zwiag AS. 2007. Evolutionary and Biomedical Insights from the Rhesus  
1045 Macaque Genome. *Science* **316**:222–234. doi:10.1126/science.1139247
- 1046 Ginestet C. 2011. ggplot2: Elegant Graphics for Data Analysis. *Journal of the Royal Statistical Society:  
1047 Series A (Statistics in Society)* **174**:245–246. doi:[https://doi.org/10.1111/j.1467-985X.2010.00676\\_9.x](https://doi.org/10.1111/j.1467-985X.2010.00676_9.x)
- 1048 Glinisky GV. 2015. Transposable Elements and DNA Methylation Create in Embryonic Stem Cells Human-  
1049 Specific Regulatory Sequences Associated with Distal Enhancers and Noncoding RNAs. *Genome Biol Evol*  
1050 **7**:1432–1454. doi:10.1093/gbe/evv081
- 1051 Göke J, Lu X, Chan Y-S, Ng H-H, Ly L-H, Sachs F, Szczerbinska I. 2015. Dynamic Transcription of Distinct  
1052 Classes of Endogenous Retroviral Elements Marks Specific Populations of Early Human Embryonic Cells.  
1053 *Cell Stem Cell* **16**:135–141. doi:10.1016/j.stem.2015.01.005
- 1054 Goodchild NL, Wilkinson DA, Mager DL. 1993. Recent Evolutionary Expansion of a Subfamily of RTVL-H  
1055 Human Endogenous Retrovirus-like Elements. *Virology* **196**:778–788. doi:10.1006/viro.1993.1535
- 1056 Gouy M, Guindon S, Gascuel O. 2010. SeaView Version 4: A Multiplatform Graphical User Interface for  
1057 Sequence Alignment and Phylogenetic Tree Building. *Molecular Biology and Evolution* **27**:221–224.  
1058 doi:10.1093/molbev/msp259
- 1059 Haig D. 2016. Transposable elements: Self-seekers of the germline, team-players of the soma. *BioEssays*  
1060 **38**:1158–1166. doi:10.1002/bies.201600125
- 1061 Heinz S, Benner C, Spann N, Bertolino E, Lin YC, Laslo P, Cheng JX, Murre C, Singh H, Glass CK. 2010.  
1062 Simple combinations of lineage-determining transcription factors prime cis-regulatory elements  
1063 required for macrophage and B cell identities. *Mol Cell* **38**:576–589. doi:10.1016/j.molcel.2010.05.004
- 1064 Hermant C, Torres-Padilla M-E. 2021. TFs for TEs: the transcription factor repertoire of mammalian  
1065 transposable elements. *Genes Dev* **35**:22–39. doi:10.1101/gad.344473.120
- 1066 Imbeault M, Helleboid P-Y, Trono D. 2017. KRAB zinc-finger proteins contribute to the evolution of gene  
1067 regulatory networks. *Nature* **543**:550–554. doi:10.1038/nature21683
- 1068 Ito J, Sugimoto R, Nakaoka H, Yamada S, Kimura T, Hayano T, Inoue I. 2017. Systematic identification and  
1069 characterization of regulatory elements derived from human endogenous retroviruses. *PLOS Genetics*  
1070 **13**:e1006883. doi:10.1371/journal.pgen.1006883
- 1071 Izsvák Z, Wang J, Singh M, Mager DL, Hurst LD. 2016. Pluripotency and the endogenous retrovirus  
1072 HERVH: Conflict or serendipity? *BioEssays* **38**:109–117. doi:10.1002/bies.201500096
- 1073 Jacobs FM, Greenberg D, Nguyen N, Haeussler M, Ewing AD, Katzman S, Paten B, Salama SR, Haussler D.  
1074 2014. An evolutionary arms race between KRAB zinc finger genes 91/93 and SVA/L1 retrotransposons.  
1075 *Nature* **516**:242–245. doi:10.1038/nature13760
- 1076 Jacques P-É, Jeyakani J, Bourque G. 2013. The Majority of Primate-Specific Regulatory Sequences Are  
1077 Derived from Transposable Elements. *PLOS Genetics* **9**:e1003504. doi:10.1371/journal.pgen.1003504
- 1078 Jern P, Sperber GO, Ahlsén G, Blomberg J. 2005. Sequence Variability, Gene Structure, and Expression of  
1079 Full-Length Human Endogenous Retrovirus H. *Journal of Virology* **79**.



- 1080 Jern P, Sperber GO, Blomberg J. 2004. Definition and variation of human endogenous retrovirus H.  
1081 *Virology* **327**:93–110. doi:10.1016/j.virol.2004.06.023
- 1082 Jetzt AE, Yu H, Klarmann GJ, Ron Y, Preston BD, Dougherty JP. 2000. High rate of recombination  
1083 throughout the human immunodeficiency virus type 1 genome. *J Virol* **74**:1234–1240.  
1084 doi:10.1128/jvi.74.3.1234-1240.2000
- 1085 Johnson WE. 2019. Origins and evolutionary consequences of ancient endogenous retroviruses. *Nat Rev*  
1086 *Microbiol* **17**:355–370. doi:10.1038/s41579-019-0189-2
- 1087 Kalkan T, Smith A. 2014. Mapping the route from naive pluripotency to lineage specification.  
1088 *Philosophical Transactions of the Royal Society B: Biological Sciences* **369**:20130540.  
1089 doi:10.1098/rstb.2013.0540
- 1090 Kelley D, Rinn J. 2012. Transposable elements reveal a stem cell-specific class of long noncoding RNAs.  
1091 *Genome Biology* **13**:R107. doi:10.1186/gb-2012-13-11-r107
- 1092 Kent WJ, Sugnet CW, Furey TS, Roskin KM, Pringle TH, Zahler AM, Haussler and D. 2002. The Human  
1093 Genome Browser at UCSC. *Genome Res* **12**:996–1006. doi:10.1101/gr.229102
- 1094 Khan H, Smit A, Boissinot S. 2006. Molecular evolution and tempo of amplification of human LINE-1  
1095 retrotransposons since the origin of primates. *Genome Res* **16**:78–87. doi:10.1101/gr.4001406
- 1096 Kinoshita M, Barber M, Mansfield W, Cui Y, Spindlow D, Stirparo GG, Dietmann S, Nichols J, Smith A.  
1097 2021. Capture of Mouse and Human Stem Cells with Features of Formative Pluripotency. *Cell Stem Cell*  
1098 **28**:453-471.e8. doi:10.1016/j.stem.2020.11.005
- 1099 Kojima KK. 2018. Human transposable elements in Repbase: genomic footprints from fish to humans.  
1100 *Mobile DNA* **9**:2. doi:10.1186/s13100-017-0107-y
- 1101 Kong Y, Rose CM, Cass AA, Williams AG, Darwish M, Lianoglou S, Haverty PM, Tong A-J, Blanchette C,  
1102 Albert ML, Mellman I, Bourgon R, Grealley J, Jhunjhunwala S, Chen-Harris H. 2019. Transposable element  
1103 expression in tumors is associated with immune infiltration and increased antigenicity. *Nat Commun*  
1104 **10**:5228. doi:10.1038/s41467-019-13035-2
- 1105 Krönung SK, Beyer U, Chiaramonte ML, Dolfini D, Mantovani R, Dobbstein M. 2016. LTR12 promoter  
1106 activation in a broad range of human tumor cells by HDAC inhibition. *Oncotarget* **7**:33484–33497.  
1107 doi:10.18632/oncotarget.9255
- 1108 Kunarso G, Chia N-Y, Jeyakani J, Hwang C, Lu X, Chan Y-S, Ng H-H, Bourque G. 2010. Transposable  
1109 elements have rewired the core regulatory network of human embryonic stem cells. *Nature Genetics*  
1110 **42**:631–634. doi:10.1038/ng.600
- 1111 Lai MM. 1992. RNA recombination in animal and plant viruses. *Microbiol Rev* **56**:61–79.
- 1112 Lanciano S, Cristofari G. 2020. Measuring and interpreting transposable element expression. *Nat Rev*  
1113 *Genet* **21**:721–736. doi:10.1038/s41576-020-0251-y
- 1114 Leigh JW, Bryant D. 2015. popart: full-feature software for haplotype network construction. *Methods in*  
1115 *Ecology and Evolution* **6**:1110–1116. doi:https://doi.org/10.1111/2041-210X.12410

- 1116 Locke DP, Hillier LW, Warren WC, Worley KC, Nazareth LV, Muzny DM, Yang S-P, Wang Z, Chinwalla AT,  
1117 Minx P, Mitreva M, Cook L, Delehaunty KD, Fronick C, Schmidt H, Fulton LA, Fulton RS, Nelson JO,  
1118 Magrini V, Pohl C, Graves TA, Markovic C, Cree A, Dinh HH, Hume J, Kovar CL, Fowler GR, Lunter G,  
1119 Meader S, Heger A, Ponting CP, Marques-Bonet T, Alkan C, Chen L, Cheng Z, Kidd JM, Eichler EE, White S,  
1120 Searle S, Vilella AJ, Chen Y, Flicek P, Ma J, Raney B, Suh B, Burhans R, Herrero J, Haussler D, Faria R,  
1121 Fernando O, Darré F, Farré D, Gazave E, Oliva M, Navarro A, Roberto R, Capozzi O, Archidiacono N, Valle  
1122 GD, Purgato S, Rocchi M, Konkel MK, Walker JA, Ullmer B, Batzer MA, Smit AFA, Hubley R, Casola C,  
1123 Schrider DR, Hahn MW, Quesada V, Puente XS, Ordoñez GR, López-Otín C, Vinar T, Brejova B, Ratan A,  
1124 Harris RS, Miller W, Kosiol C, Lawson HA, Taliwal V, Martins AL, Siepel A, RoyChoudhury A, Ma X,  
1125 Degenhardt J, Bustamante CD, Gutenkunst RN, Mailund T, Dutheil JY, Hobolth A, Schierup MH, Ryder  
1126 OA, Yoshinaga Y, de Jong PJ, Weinstock GM, Rogers J, Mardis ER, Gibbs RA, Wilson RK. 2011.  
1127 Comparative and demographic analysis of orang-utan genomes. *Nature* **469**:529–533.  
1128 doi:10.1038/nature09687
- 1129 Loewer S, Cabili MN, Guttman M, Loh Y-H, Thomas K, Park IH, Garber M, Curran M, Onder T, Agarwal S,  
1130 Manos PD, Datta S, Lander ES, Schlaeger TM, Daley GQ, Rinn JL. 2010. Large intergenic non-coding RNA-  
1131 RoR modulates reprogramming of human induced pluripotent stem cells. *Nat Genet* **42**:1113–1117.  
1132 doi:10.1038/ng.710
- 1133 Löytynoja A, Goldman N. 2010. webPRANK: a phylogeny-aware multiple sequence aligner with  
1134 interactive alignment browser. *BMC Bioinformatics* **11**:579–579. doi:10.1186/1471-2105-11-579
- 1135 Lu X, Sachs F, Ramsay L, Jacques P-É, Göke J, Bourque G, Ng H-H. 2014. The retrovirus HERVH is a long  
1136 noncoding RNA required for human embryonic stem cell identity. *Nature Structural & Molecular Biology*  
1137 **21**:423–425. doi:10.1038/nsmb.2799
- 1138 Macfarlan TS, Gifford WD, Driscoll S, Lettieri K, Rowe HM, Bonanomi D, Firth A, Singer O, Trono D, Pfaff  
1139 SL. 2012. Embryonic stem cell potency fluctuates with endogenous retrovirus activity. *Nature* **487**:57–  
1140 63. doi:10.1038/nature11244
- 1141 Mager DL, Freeman JD. 1995. HERV-H Endogenous Retroviruses: Presence in the New World Branch but  
1142 Amplification in the Old World Primate Lineage. *Virology* **213**:395–404. doi:10.1006/viro.1995.0012
- 1143 Mager DL, Freeman JD. 1987. Human endogenous retroviruslike genome with type C pol sequences and  
1144 gag sequences related to human T-cell lymphotropic viruses. *J Virol* **61**:4060–4066.  
1145 doi:10.1128/jvi.61.12.4060-4066.1987
- 1146 Matsuda E, Garfinkel DJ. 2009. Posttranslational interference of Ty1 retrotransposition by antisense  
1147 RNAs. *Proc Natl Acad Sci U S A* **106**:15657–15662. doi:10.1073/pnas.0908305106
- 1148 Miao B, Fu S, Lyu C, Gontarz P, Wang T, Zhang B. 2020. Tissue-specific usage of transposable element-  
1149 derived promoters in mouse development. *Genome Biol* **21**:1–25. doi:10.1186/s13059-020-02164-3
- 1150 Miga KH, Newton Y, Jain M, Altemose N, Willard HF, Kent WJ. 2014. Centromere reference models for  
1151 human chromosomes X and Y satellite arrays. *Genome Res* **24**:697–707. doi:10.1101/gr.159624.113
- 1152 Nakamura T, Yamada KD, Tomii K, Katoh K. 2018. Parallelization of MAFFT for large-scale multiple  
1153 sequence alignments. *Bioinformatics* **34**:2490–2492. doi:10.1093/bioinformatics/bty121

- 1154 Nichols J, Smith A. 2009. Naive and Primed Pluripotent States. *Cell Stem Cell* **4**:487–492.  
1155 doi:10.1016/j.stem.2009.05.015
- 1156 Niwa H. 2007. How is pluripotency determined and maintained? *Development* **134**:635–646.  
1157 doi:10.1242/dev.02787
- 1158 Niwa H, Nakamura A, Urata M, Shirae-Kurabayashi M, Kuraku S, Russell S, Ohtsuka S. 2016. The  
1159 evolutionally-conserved function of group B1 Sox family members confers the unique role of Sox2 in  
1160 mouse ES cells. *BMC Evolutionary Biology* **16**:173. doi:10.1186/s12862-016-0755-4
- 1161 Ohnuki M, Tanabe K, Sutou K, Teramoto I, Sawamura Y, Narita M, Nakamura Michiko, Tokunaga Y,  
1162 Nakamura Masahiro, Watanabe A, Yamanaka S, Takahashi K. 2014. Dynamic regulation of human  
1163 endogenous retroviruses mediates factor-induced reprogramming and differentiation potential. *PNAS*  
1164 **111**:12426–12431. doi:10.1073/pnas.1413299111
- 1165 Patro R, Duggal G, Love MI, Irizarry RA, Kingsford C. 2017. Salmon provides fast and bias-aware  
1166 quantification of transcript expression. *Nat Methods* **14**:417–419. doi:10.1038/nmeth.4197
- 1167 Peaston AE, Evsikov AV, Graber JH, Vries WN de, Holbrook AE, Solter D, Knowles BB. 2004.  
1168 Retrotransposons Regulate Host Genes in Mouse Oocytes and Preimplantation Embryos. *Developmental*  
1169 *Cell* **7**:597–606. doi:10.1016/j.devcel.2004.09.004
- 1170 Pérez-Losada M, Arenas M, Galán JC, Palero F, González-Candelas F. 2015. Recombination in viruses:  
1171 Mechanisms, methods of study, and evolutionary consequences. *Infect Genet Evol* **30**:296–307.  
1172 doi:10.1016/j.meegid.2014.12.022
- 1173 Pontis J, Planet E, Offner S, Turelli P, Duc J, Coudray A, Theunissen TW, Jaenisch R, Trono D. 2019.  
1174 Hominoid-Specific Transposable Elements and KZFPs Facilitate Human Embryonic Genome Activation  
1175 and Control Transcription in Naive Human ESCs. *Cell Stem Cell* **24**:724-735.e5.  
1176 doi:10.1016/j.stem.2019.03.012
- 1177 Posada D, Crandall KA. 2001. Intraspecific gene genealogies: trees grafting into networks. *Trends in*  
1178 *Ecology & Evolution* **16**:37–45. doi:10.1016/S0169-5347(00)02026-7
- 1179 Quinlan AR, Hall IM. 2010. BEDTools: a flexible suite of utilities for comparing genomic features.  
1180 *Bioinformatics* **26**:841–842. doi:10.1093/bioinformatics/btq033
- 1181 Ramírez F, Ryan DP, Grüning B, Bhardwaj V, Kilpert F, Richter AS, Heyne S, Dündar F, Manke T. 2016.  
1182 deepTools2: a next generation web server for deep-sequencing data analysis. *Nucleic Acids Research*  
1183 **44**:W160–W165. doi:10.1093/nar/gkw257
- 1184 Raney BJ, Dreszer TR, Barber GP, Clawson H, Fujita PA, Wang T, Nguyen N, Paten B, Zweig AS, Karolchik  
1185 D, Kent WJ. 2014. Track data hubs enable visualization of user-defined genome-wide annotations on the  
1186 UCSC Genome Browser. *Bioinformatics* **30**:1003–1005. doi:10.1093/bioinformatics/btt637
- 1187 Rebollo R, Romanish MT, Mager DL. 2012. Transposable elements: an abundant and natural source of  
1188 regulatory sequences for host genes. *Annu Rev Genet* **46**:21–42. doi:10.1146/annurev-genet-110711-  
1189 155621



- 1190 Römer C, Singh M, Hurst LD, Izsvák Z. 2017. How to tame an endogenous retrovirus: HERVH and the  
1191 evolution of human pluripotency. *Current Opinion in Virology*, Animal models for viral diseases •  
1192 Paleovirology **25**:49–58. doi:10.1016/j.coviro.2017.07.001
- 1193 Rossant J, Tam PPL. 2017. New Insights into Early Human Development: Lessons for Stem Cell Derivation  
1194 and Differentiation. *Cell Stem Cell* **20**:18–28. doi:10.1016/j.stem.2016.12.004
- 1195 Santoni FA, Guerra J, Luban J. 2012. HERV-H RNA is abundant in human embryonic stem cells and a  
1196 precise marker for pluripotency. *Retrovirology* **9**:111. doi:10.1186/1742-4690-9-111
- 1197 Scally A, Dutheil JY, Hillier LW, Jordan GE, Goodhead I, Herrero J, Hobolth A, Lappalainen T, Mailund T,  
1198 Marques-Bonet T, McCarthy S, Montgomery SH, Schwalie PC, Tang YA, Ward MC, Xue Y, Yngvadottir B,  
1199 Alkan C, Andersen LN, Ayub Q, Ball EV, Beal K, Bradley BJ, Chen Y, Clee CM, Fitzgerald S, Graves TA, Gu Y,  
1200 Heath P, Heger A, Karakoc E, Kolb-Kokocinski A, Laird GK, Lunter G, Meader S, Mort M, Mullikin JC,  
1201 Munch K, O'Connor TD, Phillips AD, Prado-Martinez J, Rogers AS, Sajjadian S, Schmidt D, Shaw K,  
1202 Simpson JT, Stenson PD, Turner DJ, Vigilant L, Vilella AJ, Whitener W, Zhu B, Cooper DN, de Jong P,  
1203 Dermitzakis ET, Eichler EE, Flicek P, Goldman N, Mundy NI, Ning Z, Odom DT, Ponting CP, Quail MA,  
1204 Ryder OA, Searle SM, Warren WC, Wilson RK, Schierup MH, Rogers J, Tyler-Smith C, Durbin R. 2012.  
1205 Insights into hominid evolution from the gorilla genome sequence. *Nature* **483**:169–175.  
1206 doi:10.1038/nature10842
- 1207 Schön U, Seifarth W, Baust C, Hohenadl C, Erfle V, Leib-Mösch C. 2001. Cell Type-Specific Expression and  
1208 Promoter Activity of Human Endogenous Retroviral Long Terminal Repeats. *Virology* **279**:280–291.  
1209 doi:10.1006/viro.2000.0712
- 1210 Simon-Loriere E, Holmes EC. 2011. Why do RNA viruses recombine? *Nat Rev Microbiol* **9**:617–626.  
1211 doi:10.1038/nrmicro2614
- 1212 Smit AF, Hubley R, Green P. 2013. RepeatMasker Open-4.0.
- 1213 Storer J, Hubley R, Rosen J, Wheeler TJ, Smit AF. 2021. The Dfam community resource of transposable  
1214 element families, sequence models, and genome annotations. *Mobile DNA* **12**:2. doi:10.1186/s13100-  
1215 020-00230-y
- 1216 Sundaram V, Cheng Y, Ma Z, Li D, Xing X, Edge P, Snyder MP, Wang T. 2014. Widespread contribution of  
1217 transposable elements to the innovation of gene regulatory networks. *Genome Res* **24**:1963–1976.  
1218 doi:10.1101/gr.168872.113
- 1219 Sundaram V, Wysocka J. 2020. Transposable elements as a potent source of diverse cis-regulatory  
1220 sequences in mammalian genomes. *Philosophical Transactions of the Royal Society B: Biological Sciences*  
1221 **375**:20190347. doi:10.1098/rstb.2019.0347
- 1222 Svoboda P, Stein P, Anger M, Bernstein E, Hannon GJ, Schultz RM. 2004. RNAi and expression of  
1223 retrotransposons MuERV-L and IAP in preimplantation mouse embryos. *Developmental Biology*  
1224 **269**:276–285. doi:10.1016/j.ydbio.2004.01.028
- 1225 Takahashi K, Nakamura M, Okubo C, Kliesmete Z, Ohnuki M, Narita M, Watanabe A, Ueda M, Takashima  
1226 Y, Hellmann I, Yamanaka S. 2021. The pluripotent stem cell-specific transcript ESRG is dispensable for  
1227 human pluripotency. *PLOS Genetics* **17**:e1009587. doi:10.1371/journal.pgen.1009587

- 1228 Tang F, Barbacioru C, Bao S, Lee C, Nordman E, Wang X, Lao K, Surani MA. 2010. Tracing the Derivation  
1229 of Embryonic Stem Cells from the Inner Cell Mass by Single-Cell RNA-Seq Analysis. *Cell Stem Cell* **6**:468–  
1230 478. doi:10.1016/j.stem.2010.03.015
- 1231 Theunissen TW, Friedli M, He Y, Planet E, O’Neil RC, Markoulaki S, Pontis J, Wang H, Iouranova A,  
1232 Imbeault M, Duc J, Cohen MA, Wert KJ, Castanon R, Zhang Z, Huang Y, Nery JR, Drotar J, Lungjangwa T,  
1233 Trono D, Ecker JR, Jaenisch R. 2016. Molecular Criteria for Defining the Naive Human Pluripotent State.  
1234 *Cell Stem Cell* **19**:502–515. doi:10.1016/j.stem.2016.06.011
- 1235 Thomas J, Perron H, Feschotte C. 2018. Variation in proviral content among human genomes mediated  
1236 by LTR recombination. *Mobile DNA* **9**:36. doi:10.1186/s13100-018-0142-3
- 1237 Thompson PJ, Macfarlan TS, Lorincz MC. 2016. Long Terminal Repeats: From Parasitic Elements to  
1238 Building Blocks of the Transcriptional Regulatory Repertoire. *Molecular Cell* **62**:766–776.  
1239 doi:10.1016/j.molcel.2016.03.029
- 1240 Urusov FA, Nefedova LN, Kim AI. 2011. Analysis of the tissue- and stage-specific transportation of the  
1241 *Drosophila melanogaster* gypsy retrotransposon. *Russ J Genet Appl Res* **1**:507–510.  
1242 doi:10.1134/S2079059711060104
- 1243 Vargiu L, Rodriguez-Tomé P, Sperber GO, Cadeddu M, Grandi N, Blikstad V, Tramontano E, Blomberg J.  
1244 2016. Classification and characterization of human endogenous retroviruses; mosaic forms are common.  
1245 *Retrovirology* **13**:7. doi:10.1186/s12977-015-0232-y
- 1246 Wang J, Xie G, Singh M, Ghanbarian AT, Raskó T, Szvetnik A, Cai H, Besser D, Prigione A, Fuchs NV,  
1247 Schumann GG, Chen W, Lorincz MC, Ivics Z, Hurst LD, Izsvák Z. 2014. Primate-specific endogenous  
1248 retrovirus-driven transcription defines naive-like stem cells. *Nature* **516**:405–409.  
1249 doi:10.1038/nature13804
- 1250 Wang Z, Oron E, Nelson B, Razis S, Ivanova N. 2012. Distinct lineage specification roles for NANOG,  
1251 OCT4, and SOX2 in human embryonic stem cells. *Cell Stem Cell* **10**:440–454.  
1252 doi:10.1016/j.stem.2012.02.016
- 1253 Waterhouse AM, Procter JB, Martin DMA, Clamp M, Barton GJ. 2009. Jalview Version 2—a multiple  
1254 sequence alignment editor and analysis workbench. *Bioinformatics* **25**:1189–1191.  
1255 doi:10.1093/bioinformatics/btp033
- 1256 Waterson RH, Lander ES, Wilson RK, The Chimpanzee Sequencing and Analysis Consortium. 2005. Initial  
1257 sequence of the chimpanzee genome and comparison with the human genome. *Nature* **437**:69–87.  
1258 doi:10.1038/nature04072
- 1259 Wolf G, de Iaco A, Sun M-A, Bruno M, Tinkham M, Hoang D, Mitra A, Ralls S, Trono D, Macfarlan TS.  
1260 2020. KRAB-zinc finger protein gene expansion in response to active retrotransposons in the murine  
1261 lineage. *eLife* **9**:e56337. doi:10.7554/eLife.56337
- 1262 Yang P, Wang Y, Macfarlan TS. 2017. The role of KRAB-ZFPs in transposable element repression and  
1263 mammalian evolution. *Trends Genet* **33**:871–881. doi:10.1016/j.tig.2017.08.006

- 1264 Yu H-L, Zhao Z-K, Zhu F. 2013. The role of human endogenous retroviral long terminal repeat sequences  
1265 in human cancer (Review). *International Journal of Molecular Medicine* **32**:755–762.  
1266 doi:10.3892/ijmm.2013.1460
- 1267 Zhang Y, Li T, Preissl S, Amaral ML, Grinstein JD, Farah EN, Destici E, Qiu Y, Hu R, Lee AY, Chee S, Ma K, Ye  
1268 Z, Zhu Q, Huang H, Fang R, Yu L, Izpisua Belmonte JC, Wu J, Evans SM, Chi NC, Ren B. 2019.  
1269 Transcriptionally active HERV-H retrotransposons demarcate topologically associating domains in human  
1270 pluripotent stem cells. *Nature Genetics* **51**:1380–1388. doi:10.1038/s41588-019-0479-7
- 1271